Distinct Stromal Cell Populations Define the B-cell Acute Lymphoblastic Leukemia Microenvironment

Mauricio N. Ferrao Blanco[1], Bexultan Kazybay[1], Mirjam Belderbos[1], Olaf Heidenreich[1], Hermann Josef Vormoor[1,2]

[1] Princess Máxima Center for Pediatric Oncology, Utrecht, the Netherlands
[2] University Medical Center Utrecht, Utrecht, the Netherlands

Abstract

The bone marrow microenvironment plays a critical role in B-cell acute lymphoblastic leukemia (B-ALL) progression, yet its cellular heterogeneity remains poorly understood. Using single-cell RNA sequencing on patient-derived of bone marrow aspirates from pediatric B-ALL patients, we identified two distinct mesenchymal stromal cell (MSC) populations: early mesenchymal progenitors and adipogenic progenitors. Spatial transcriptomic analysis further revealed the localization of these cell types and identified a third stromal population, osteogenic-lineage cells, exclusively present in the bone biopsy. Functional *ex vivo* assays using sorted stromal populations derived from B-ALL patient bone marrow aspirates demonstrated that both early mesenchymal and adipogenic progenitors secrete key niche-supportive factors, including CXCL12 and Osteopontin, and support leukemic cell survival and chemoresistance. Transcriptomic profiling revealed that B-ALL cells interact differently with stromal subtypes. Notably, adipogenic progenitors, but not early mesenchymal progenitors, provide support to leukemic cells through interleukin-7 and VCAM1 signaling. Stromal cells from B-ALL patients exhibited an enhanced adipogenic differentiation capacity compared to healthy controls. Moreover, co-culture experiments showed that B-ALL cells induce adipogenic differentiation in healthy MSCs through a cell contact-dependent mechanism. Adipogenic progenitors were also enriched in relapse samples, implicating them in disease progression. These findings highlight the complexity of the B-ALL microenvironment and identify different specialized stromal niches with which the leukemic cells can engage.

Introduction

The bone marrow microenvironment is a highly specialized tissue consisting of different cell types and extracellular matrix proteins, essential for regulating hematopoiesis and skeletal

regeneration [1]. Central to this intricate network are mesenchymal stromal cells (MSCs), a heterogeneous population encompassing multipotent progenitors of skeletal lineages [2, 3]. These MSCs contribute to the formation of specialized niches within the bone marrow, which provide essential support for hematopoietic stem cell (HSC) function, including homing, quiescence, and lineage commitment [4-6].

The dynamic interplay between leukemic cells and the bone marrow microenvironment is increasingly recognized as a critical factor in hematological malignancies, including B-cell acute lymphoblastic leukemia (B-ALL) [7]. Leukemic cells actively reprogram their microenvironment to create a supportive niche that promotes survival, proliferation, and resistance to therapy [8-10]. While previous studies have implicated a key role of the bone marrow microenvironment in B-ALL, a comprehensive understanding of its cellular heterogeneity remains elusive.

To address this knowledge gap, we conducted a comprehensive single-cell RNA sequencing analysis of the bone marrow microenvironment in pediatric B-ALL. By systematically characterizing the stromal, hematopoietic, and leukemic compartments, we identified distinct MSC populations as key contributors to the leukemia-supportive niche. Notably, our findings reveal a previously unrecognized role for adipogenic progenitors in the leukemic niche and shed light on the complexity of the cellular micro-environment in B-ALL.

Results

The single cell bone marrow landscape of B-ALL

To comprehensively characterize the bone marrow microenvironment in B-ALL, we employed flow cytometry to isolate leukemic plus normal B-lineage (CD19+), non-leukemic hematopoietic (CD45+CD235a+), and non-hematopoietic (CD19-CD45-CD235a-) mononuclear cells from patient bone marrow aspirates (Figure 1A). The identity of the non-hematopoietic fraction was confirmed by its ability to form colony-forming unit fibroblasts (CFU-Fs), express MSC markers (CD90, CD73, CD105), and differentiate into adipocytes and osteoblasts (Supplementary Figure 1). We analyzed bone marrow mononuclear cells from nine B-ALL patients, encompassing 5 different molecular subtypes as well as samples taken at diagnosis and relapse (Figure 1B; Supplementary Table 1). A healthy donor sample from an

65 18-year-old woman was included in the scRNA-seq analysis and only the non-hematopoietic
66 compartment from this sample was sorted and sequenced. After quality control and doublet
67 exclusion, 28,333 high-quality cells were obtained and integrated into a single dataset for
68 further analysis. We generated a single-cell transcriptomic map of the integrated stromal,
69 hematopoietic, and leukemic compartment (Figure 1C). We observe variable contribution of
70 each patient to each cluster (Figure 1D), though given our small cohort (n=9), an association
71 with molecular subtype, age and sex is not feasible. Unsupervised clustering identified twenty
72 major cell populations based on the expression of lineage-specific markers (Figure 1E;
73 Supplementary Table 2). These clusters included, among others, stromal cells (expressing
74 *CXCL12*, *THY1* and *FN1*), mature B cells (expressing *CD19*, *CD22* and *MS4A1*) and leukemic
75 cells (expressing *CD19*, *CD22* and *MME*). The expression of CD19 was relatively low, which
76 could be associated to technical limitations of scRNAseq, such as high proportion of zero
77 counts resulting from low sequencing depth [11], the lower stability of mRNA compared to
78 protein, or biological factors including acquired mutations or alternative splicing [12, 13].
79 Expression of the hematopoietic marker *PTPRC,* which encodes CD45*,* was ubiquitous except
80 in erythroblasts and stromal cells. Further discrimination between leukemic and mature B
81 cells was based on the aberrant karyotype of ALL cells, inferred by copy number variation
82 analysis (Supplementary Figure 2). Unbiased cell type recognition using bone marrow
83 scRNAseq references [14, 15], confirmed the cell annotation and mapped leukemic cells to
84 pro-B and preproB-cells, confirming their immature phenotype (Supplementary Figure 3).
85 Gene ontology enrichment analysis validated the cellular identity of each cluster, for example,
86 stromal cells were enriched in genes associated with collagen-containing extracellular matrix,
87 while T cells were enriched in express genes associated with T cell activation (Supplementary
88 Figure 4).
89 In summary, the data presented here provide a comprehensive single-cell transcriptomic
90 blueprint of the bone marrow microenvironment in pediatric B-ALL.
91

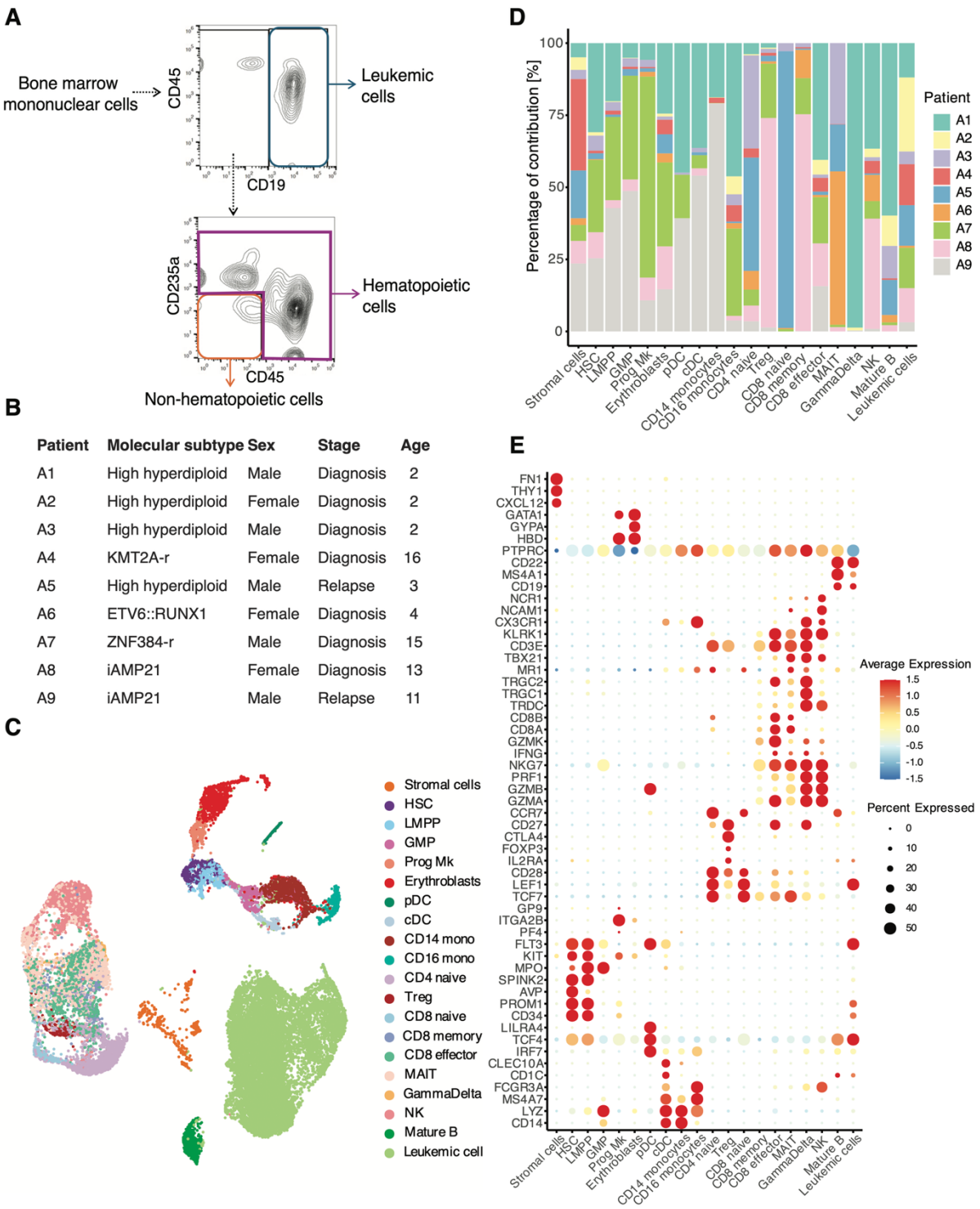

Figure 1. Integrated analysis of the B-ALL bone marrow microenvironment. A) Gating strategy for the enrichment of leukemic cells plus normal B-lineage cells (CD19+), hematopoietic cells (CD45+CD235a+) and non-hematopoietic cells (negative for all markers). B) Table detailing the molecular subtype, age and sex associated with each sample sequenced. C) Uniform Manifold Approximation and Projection (UMAP) plot showing cell clusters from the analysis

99 of 28,333 cells integrated from 9 patient samples. D) Barplot indicating the contribution of
100 individual patients to each cell cluster. E) DotPlot representation of gene expression of typical
101 cell cluster markers, 3 markers per cluster. The size of the dot indicates the percentage of
102 cells expressing the gene and the color indicates the average expression level. Abbreviations.
103 Lymphoid-primed multipotent progenitors (LMPP), megakaryocyte progenitors (Prog Mk),
104 granulocyte-macrophage progenitors (GMP), plasmacytoid dendritic cells (pDC), conventional
105 dendritic cells (cDC), hematopoietic stem cells (HSCs), mucosal-associated invariant T cells
106 (MAIT), regulatory T cells (Tregs), natural killer cells (NK).
107

108 ## Identification of distinct stromal cell populations
109

110 The stromal landscape in B-ALL remains largely unexplored. In-depth analysis of the stromal
111 cell cluster revealed two distinct populations: early mesenchymal progenitors and adipogenic
112 progenitors (Figures 2A). By comparing our data with a human bone marrow stromal cell atlas
113 [14], we mapped early mesenchymal progenitors to fibro-MSCs (Figure 2B and
114 Supplementary Figure 5). In contrast, adipogenic progenitors mapped to adipo-MSCs, which
115 resemble reported marrow adipogenic lineage precursors and Adipo-CXCL12-abundant-
116 reticular (Adipo-CAR) cells in mice [16, 17]. Accordingly, adipogenic progenitors showed high
117 expression of adipogenic markers *LPL, PPARG* and *LEPR*, while early mesenchymal progenitors
118 did not, neither markers of other stromal fate-committed cells such as osteoblasts (*IBSP,*
119 *RUNX2, BGLAP*) or chondrocytes (*SOX9*) (Figure 2D). Gene set enrichment analysis
120 demonstrated that adipogenic progenitors were enriched in extracellular matrix-related
121 genes (Figure 2C), mainly collagen type I, type III and type XII, as well as fibrillin-1 and Decorin
122 (Figure 2D).
123 To elucidate transcription factor activity of stromal cells, we assessed the activity of key
124 transcription factors using the single-cell regulatory network inference and clustering
125 (SCENIC) method [18]. Adipogenic progenitors exhibited high activity of adipogenic master
126 regulators such as EBF1 and FOSB [19, 20], while early mesenchymal progenitors showed
127 elevated ZNF580, CEBPD and ATF4 activity, associated with a more upstream progenitor state
128 [21] (Figure 2E, Supplementary Table 3). Signaling pathway analysis suggest higher MAPK,
129 PI3K and JAK/STAT signaling in adipogenic progenitors compared with early mesenchymal
130 progenitors, consistent with their role in adipogenesis [22-24] (Figure 2F). Lastly, pseudotime

analysis indicated a more primitive state for early mesenchymal progenitors compared to adipogenic progenitors (Figure 2G).

Overall, our findings delineate the transcriptomic diversity within the stromal niche in B-ALL, providing novel insights into the cellular heterogeneity of this critical microenvironment.

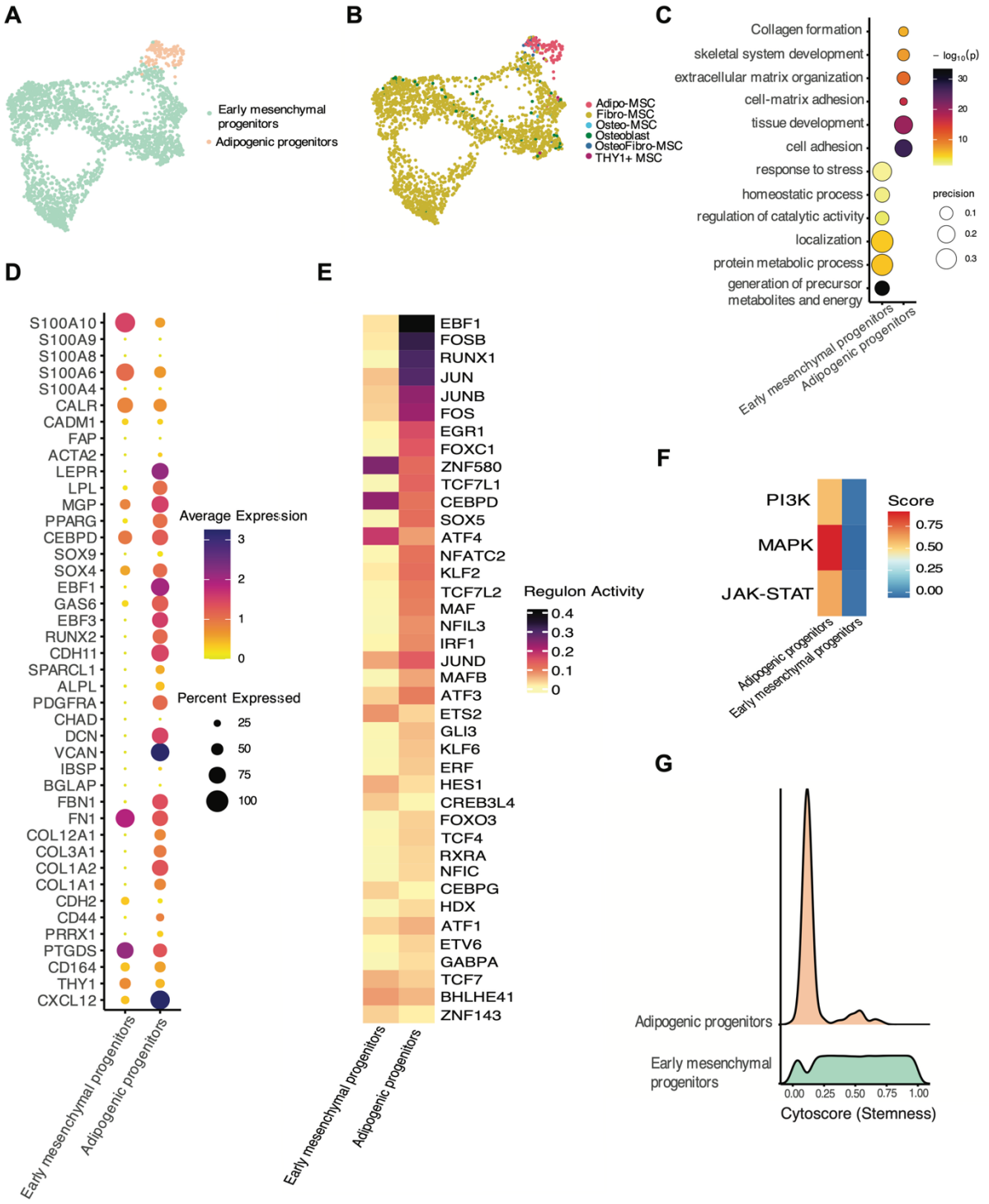

138 Figure 2. Characterization of the B-ALL stromal niche. A) UMAP representation of the stromal
139 clusters. B) UMAP plot showing the annotation after mapping the stromal cluster to the
140 reported by Bandyopadhyay et al, 2024. C) Dot plot showing enriched gene ontology (GO)
141 terms of differentially expressed genes in the cell clusters. D) Dot plot representing the gene
142 expression of selected markers in adipogenic and early mesenchymal progenitors. E)
143 Heatmap representation of transcription factor activity score inferred by SCENIC. F) Heatmap
144 depicting pathway activity analysis. G) Ridge plot showing the distribution of Cytotrace scores
145 for adipogenic and early mesenchymal progenitors. Each ridge represents a different stromal
146 cell population, with adipogenic progenitors in pink and early mesenchymal progenitors in
147 green. The x-axis represents the Cytotrace score, which reflects the differentiation trajectory
148 of cells. A higher Cytotrace score indicates a higher stemness profile. The y-axis represents
149 the density of cells at a particular Cytotrace score.
150

151 ## Spatial localization of stromal niches

152
153 We next analyzed a publicly available spatial transcriptomics dataset generated using a
154 trephine bone biopsy sample from a B-ALL patient (Xenium technology, 10x Genomics) [25].
155 Patient age, sex, or molecular subtype were not provided with the dataset. Due to the
156 limitation of the Xenium gene panel, which includes only 477 genes, a detailed annotation of
157 hematopoietic clusters- similar to that achieved in our single-cell RNA-seq analysis of bone
158 marrow aspirates- was not feasible (Supplementary Figure 6). To investigate the spatial
159 localization of stromal populations in B-ALL bone marrow, we annotated distinct stromal cell
160 types, identifying early mesenchymal progenitors, adipogenic progenitors, and osteogenic-
161 lineage cells within the sample (Figure 3A). Cell types were identified based on the expression
162 of top marker genes: adipogenic progenitors expressed high levels of LPL and FABP4,
163 osteogenic-lineage cells expressed BMP2 and IBSP, while early mesenchymal progenitors
164 lacked lineage-committed markers but expressed the extracellular matrix gene COL1A1
165 (Figure 3B). The stromal niche was predominantly composed of adipogenic progenitors, which
166 accounted for approximately 70% of the stromal cells (Figure 3C). Notably, osteogenic-lineage
167 cells- absent in our single-cell RNA seq dataset of bone marrow aspirates- were identified in
168 this spatial dataset, likely due to their strong adherence to the bone surface, making them
169 less accessible in aspirated material.

170 Interestingly, adipogenic progenitors were primarily located around blood vessels and closely
171 associated with vascular endothelial cells (Figure 3D & F). This spatial pattern suggests that at
172 least a subset of these cells may represent pericytes, which is consistent with previous murine
173 studies linking adipogenic progenitors to perivascular cells [16]. In contrast, early
174 mesenchymal progenitors were more randomly distributed throughout the marrow, while
175 osteogenic-lineage cells were predominantly located along the bone surface (Figure 3E & G).

176 A niche analysis incorporating all cell populations within the spatial transcriptomic dataset
177 revealed distinct spatial domains, underscoring the differential localization of stromal
178 populations within the B-ALL bone marrow microenvironment (Figure 3J; Supplementary
179 Figure 7). Osteogenic-lineage cells were exclusively found in **niche 4**, whereas adipogenic
180 progenitors and early mesenchymal progenitors were mainly enriched in **niche 2**, together
181 with vascular endothelial cells (Figure 3H & I).

182 These findings emphasize the spatial heterogeneity and distinct localization patterns of
183 stromal populations within the bone marrow ecosystem in B-ALL.

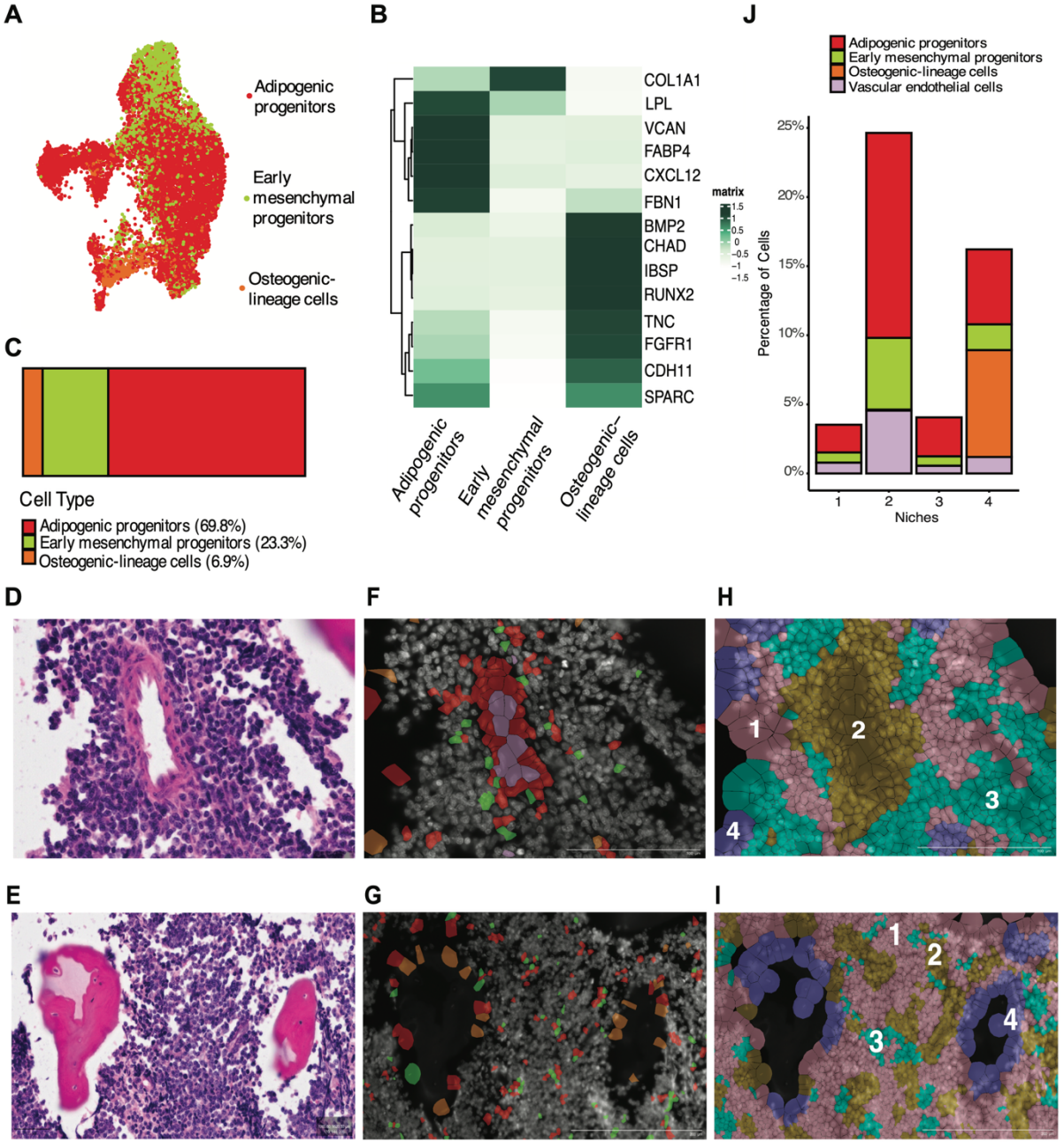

Figure 3. Spatial single-cell analysis of the B-ALL bone marrow niche. A) Uniform Manifold Approximation and Projection (UMAP) plot showing the stromal cell clusters identified in the Xenium data. B) Heatmap showing the average gene expression per cluster of selected top markers. C) Barplot representing the percentage of each stromal population relative to the total stromal cell types in the dataset. D-E) Hematoxilin & Eosin staining of the bone biopsy, zooming in a blood vessel (D) and trabelular bone (E). F-G) Localization of early mesenchymal

191 progenitors (green), adipogenic progenitors (red), osteogenic-lineage cells (brown) and
192 vascular endothelial cells (violet) on the same area as in D and E. H-I) Localization of the 4
193 different niches on the same area as in D and E. Each color represents a different niche, pink
194 (1), yellow (2), cyan (3), purple (4). J) Barplot showing the cell type distribution between the
195 four niches. In the y-axis, the percentage of these cell types relative to all the cell types
196 composing the niche is shown.
197

198 ## Functional heterogeneity of mesenchymal stromal cell populations

199

200 To further validate and functionally characterize the distinct stromal populations observed in
201 bone marrow aspirates, we developed a FACS sorting strategy based on markers identified
202 through our scRNA-seq analysis of non-cultured stromal cells (Figure 4A & 4B). Adipogenic
203 progenitors were defined by the high expression of *CDH11* (Cadherin 11) and *VCAM1* (CD106),
204 while early mesenchymal progenitors were negative for these markers and positive for CD81
205 and *THY* (CD90). Notably, commonly used MSC markers exhibited variable expression among
206 stromal subsets (Figure 4A). Flow cytometry analysis of cultured, sorted stromal populations
207 confirmed the expression patterns of these markers (Figure 4H). Cadherin 11 and CD106 were
208 detected on the surface of adipogenic progenitors (100% and 30%, respectively), while early
209 mesenchymal progenitors were negative for these markers. Conversely, CD90 was
210 consistently detected on early mesenchymal progenitors (99.5%) but was only partially
211 expressed on adipogenic progenitors (40%). CD81 was expressed on both populations (100%).
212 Both populations also exhibited strong positivity for the stromal markers CD51 and CD164
213 (>98% in both). These results highlight the importance of using a comprehensive panel of
214 markers when studying MSCs and underscore the distinct phenotypic characteristics of these
215 two stromal populations.
216 To validate our sorting strategy, we performed single-cell RNA sequencing on sorted early
217 mesenchymal and adipogenic progenitors and assessed their similarity to the sorted – non
218 cultured stromal populations signature (Figure 4C & D). By annotating the cultured stromal
219 populations using uncultured ones as a reference, we observed that 36.5% of the
220 CD106+CDH11+ cells were adipogenic progenitors in contrast to only 9.1% in case of the
221 CD81+CD90+ cells, confirming the sorting strategy for the stromal population enrichment.

Pseudotime analysis confirmed the more differentiated state of adipogenic progenitors compared to early mesenchymal progenitors (Figure 4E). Functional assays revealed a higher CFU-F formation capacity and proliferation rate in early mesenchymal progenitors, consistent with their stem/progenitor-like phenotype (Figure 4F). Conversely, adipogenic progenitors demonstrated enhanced adipogenic and osteogenic differentiation potential (Figures 4G, Supplementary Figure 8). Overall, these findings confirm the functional divergence of early mesenchymal and adipogenic progenitors.

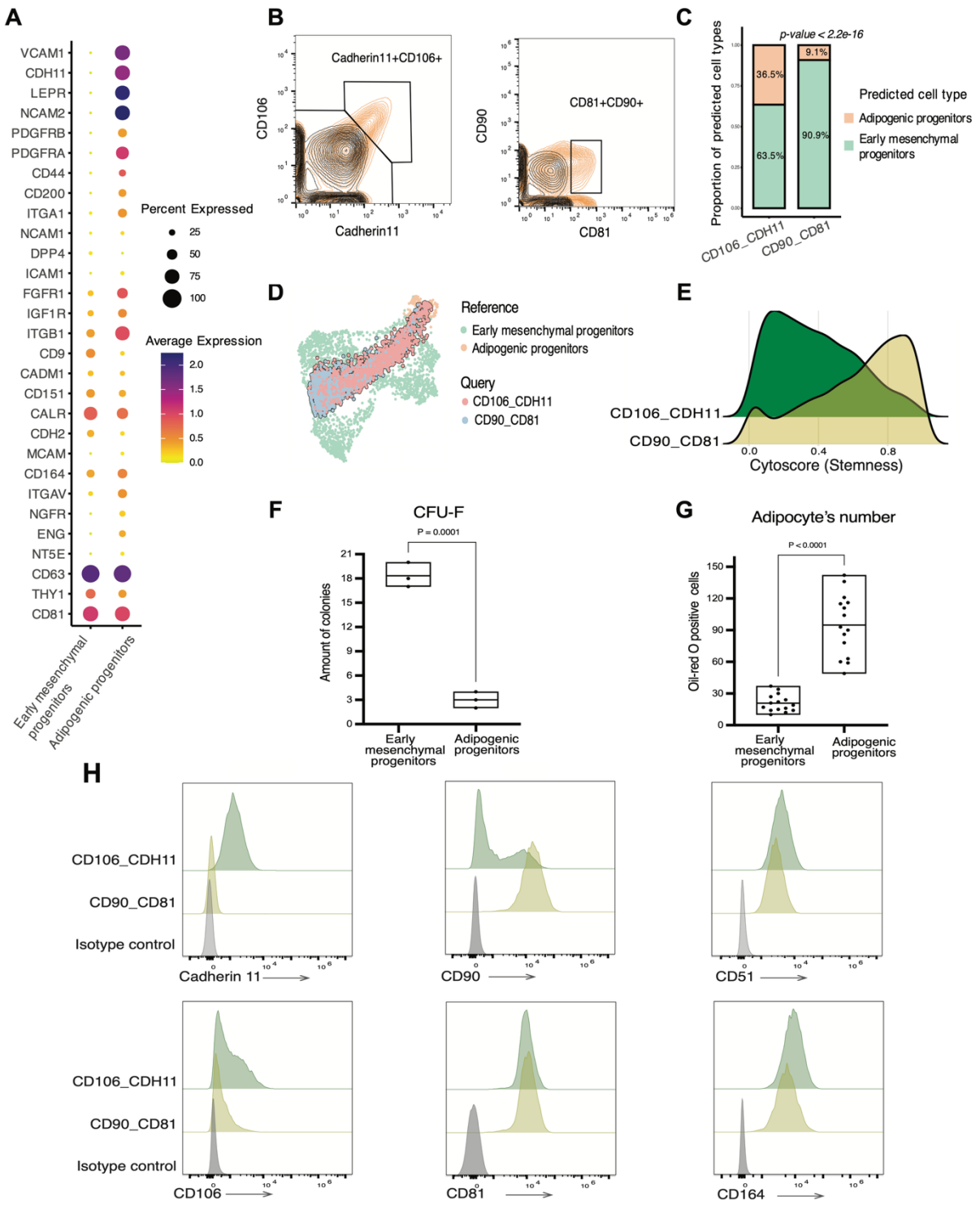

Figure 4. Functional characterization of stromal cell populations in B-ALL. A) Dotplot representation of selected cell surface markers in non-cultured early mesenchymal and adipogenic progenitors derived from bone marrow aspirates. The size of the dot indicates the percentage of cells expressing the gene and the color indicates the average expression level.

237 B) Gating strategy for the sorting of stromal populations. In black the isotype control, while in
238 orange the stained sample. C) Barplot showing the reference-based annotation of the sorted
239 cultured stromal cells, using the non-expanded stromal cells as a reference. Sorted stromal
240 cells were analyzed at passage 3. D) UMAP representation of the scRNAseq data of the two
241 cultured stromal populations projected in the reference dataset of non-expanded stromal
242 cells. E) Ridge plots of the two sorted stromal populations showing the predicted order score
243 in differentiation. Each ridge represents a different stromal cell population, with
244 CD106+CDH11+ in green and CD81+CD90+ in yellow. The x-axis represents the Cytotrace
245 score, which reflects the differentiation trajectory of cells. A higher Cytotrace score indicates
246 a higher stemness profile. The y-axis represents the density of cells at a particular Cytotrace
247 score. F) CFU-F analysis of sorted stromal populations cultured *ex vivo* at passage 3. A total of
248 475 cells per well were plated in a 6-well plate (50 cells/cm2). Colonies were quantified after
249 10 days of culture (n=3). Statistical significance was assessed by a two-tailed unpaired
250 Student's t-test. G) Stromal cells at passage 3 were cultured in adipogenic medium for 14
251 days. Oil red O stains lipid droplets (red). The number of positive cells were quantified per
252 well in a 96-well plate. Data is presented as mean ± standard deviation. Statistical significance
253 was assessed by a two-tailed unpaired Student's t-test. H) Immunophenotypic
254 characterization of cultured, sorted stromal populations at passage 3. Histograms showing
255 the fluorescence intensity of CD markers determined by flow cytometry. Signal intensity is
256 shown on the x-axis and count on the y-axis. Adipogenic progenitors are shown in green, early
257 mesenchymal progenitors in yellow and isotype controls in gray.
258

259 <u>Early mesenchymal and adipogenic progenitors support leukemic cell survival</u>
260 <u>via alternative mechanisms.</u>
261

262 Leukemic cell survival is dependent on the microenvironment [26]. To investigate whether
263 stromal heterogeneity influences the production of different supportive factors, we analyzed
264 the expression of known niche factors [26, 27]. RNA expression indicated that different MSC
265 types may produce specific support factors; for example, *SPP1* (osteopontin) and CDH2 (N-
266 Cadherin) was highest in early mesenchymal progenitors, whereas *CXCL12*, *VCAM1* (vascular

267 cell adhesion molecule-1), *ANGPT1* (angiopoietin-1), *IL7* (interleukin 7) and *KITLG* (stem cell
268 factor) were predominantly expressed by adipogenic progenitors (Figure 5A) [28] [29] [30].
269 To further explore stromal-leukemic cell interactions in an unbiased manner, we performed
270 ligand-receptor interaction analysis (Figure 5B). By quantifying the interactions of the niche
271 cells with the leukemic cells, we found that adipogenic progenitors were categorized as the
272 primary source of ligands interacting with leukemic cells, followed by early mesenchymal
273 progenitors (Figure 5C).
274 To gain a deeper understanding of the underlaying regulatory mechanisms in the complex
275 communication ecosystem, we further classified the cell-cell interactions into patterns where
276 groups of cells are grouped together if they share a similar communication pattern (Figure
277 5D). We identified 5 patterns, each of them related to a group of cells, hematopoietic
278 progenitors (pattern 1), adipogenic progenitors (pattern 2), T lymphocytes (pattern 3),
279 myeloid cells (pattern 4) and early mesenchymal progenitors (pattern 5). These patterns were
280 characterized by different interactions involving secreted factors, cell-cell contact, and
281 extracellular matrix-receptor signaling, highlighting the different mechanisms that cells use in
282 the bone marrow niche (Supplementary Figure 9). Interestingly, novel niche-ALL interactions
283 were identified, such as MIF - (CD74 + CXCR4) for early mesenchymal progenitors and Ephrin
284 A5 - EPHA7 for adipogenic progenitors.
285 To validate these findings, we performed co-culture studies using patient-derived B-ALL cells
286 with the two stromal populations. Consistent with our computational analysis, we observed
287 that both stromal populations supported *ex vivo* survival of primary ALL cells. However,
288 adipogenic progenitors exhibited a slightly stronger supportive effect compared to early
289 mesenchymal progenitors (Figure 5E). Dose-response analysis of dexamethasone showed
290 that both stromal populations provide chemoresistance to B-ALL cells (Figure 5F). Multiplex
291 cytokine analysis revealed elevated secretion of CXCL12 and osteopontin in the co-culture
292 medium of both stromal populations (Figure 5G & H). Notably, interleukin 7 and stem cell
293 factor were exclusively detected in the co-culture medium of adipogenic progenitors, aligning
294 with our transcriptomic findings (Figure 5I & J).
295

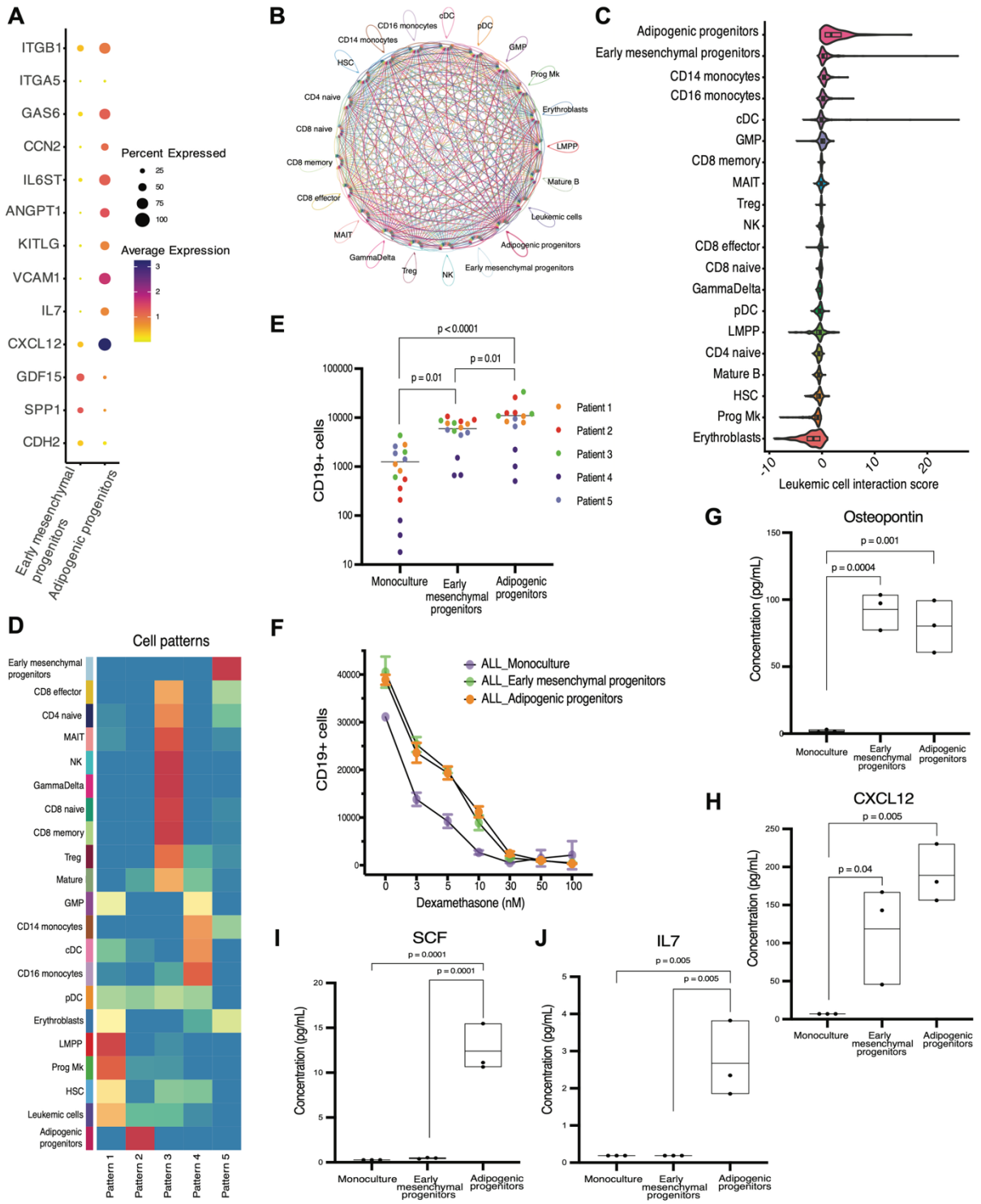

Figure 5. Cell-cell communication analysis in the B-ALL niche. A) Dotplot representation of the gene expression of widely studied niche factors. The size of the dot indicates the percentage of cells expressing the gene and the color indicates the average expression level. B) Circle plot showing the interactions between niche cell clusters and leukemic cells. The thickness of the

302 line represents the strength of the interaction. The colors of the lines represent a different
303 cell population. C) Representation of the strength of the cell-cell interaction of the niche cells
304 with the leukemic cells, calculated as a leukemic cell interaction score. The score is based on
305 the average expression of signaling factors (cytokines, integrins, extracellular matrix
306 components) that were inferred to interact with leukemic cells. D) Non-negative matrix
307 factorization (NMF) to identify modules in the cell-cell interaction pathways between niche
308 cells and leukemic cells. A total of 5 modules were identified based on Cophenetic and
309 Silhouette metrics. Clusters of cells are grouped into each module. E) Absolute number of
310 CD19+ leukemic cells per well after seven days of monoculture or co-culture with adipogenic
311 and early mesenchymal progenitors. Colors depict different patients. Data is presented as
312 mean ± standard deviation. Statistical significance was assessed by a two-way ANOVA with
313 Bonferroni's multiple comparison. F) Dose-response analysis of Dexamethasone (0 – 100 nM)
314 by quantifying the absolute number of CD19+ leukemic cells per well after seven days of
315 monoculture or co-culture with adipogenic and early mesenchymal progenitors. Cell counts
316 are shown as mean ± standard deviation of three replicates. A two-way ANOVA revealed
317 significant effects of Dex concentration (**p** $< 2 \times 10^{-16}$), cell type (**p** $< 2 \times 10^{-16}$), and their
318 interaction (**p** $= 9.81 \times 10^{-15}$). Pairwise comparisons (adjusted using the Benjamini-Hochberg
319 method) at each Dex concentration revealed significant differences between groups: 3 μM
320 Monoculture vs. AP (p = 0.015), EMP vs. AP (p = 0.035), 5 μM Monoculture vs. EMP ($p = 6.8 \times$
321 10^{-5}), Monoculture vs. AP ($p = 6.8 \times 10^{-5}$), 10 μM Monoculture vs. EMP (p = 0.00081),
322 Monoculture vs. AP (p = 0.00029), 30 μM Monoculture vs. EMP (p = 0.0077), Monoculture vs.
323 AP (p = 0.00056), EMP vs. AP (p = 0.0077). G-J) Multiplex cytokine analysis of osteopontin,
324 CXCL12, SCF and IL-7 in the medium of the co-culture experiments. Each datapoint denotes a
325 replicate sample. Statistical significance was assessed by a one-way ANOVA and Tukey's HSD
326 post-hoc test.
327

328 <u>Interleukin 7 and VCAM1 are adipogenic progenitor-specific ALL supportive</u>
329 <u>signals</u>

330 Given the distinct communication pathways identified through transcriptomic analysis by
331 which the two stromal populations support ALL cells, we sought to further investigate these
332 mechanisms *ex vivo*. We first examined whether the enhanced ALL cell survival observed in

333 co-culture with stromal populations was dependent on cytokine signaling. To this end, we
334 targeted the signaling mediated by interleukin-7, osteopontin, and CXCL12 using blocking
335 antibodies against IL7 and osteopontin, and plerixafor, an inhibitor of the CXCL12 receptor
336 CXCR4. While Plerixafor and anti-osteopontin reduced the supportive effect of both stromal
337 populations on ALL cells, anti-IL7 specifically decreased ALL cell survival in co-culture with
338 adipogenic progenitors, without affecting their survival in co-culture with early mesenchymal
339 progenitors or in monoculture (Figure 6A-C). These findings align with the specific secretion
340 of IL7 predominantly by adipogenic progenitors, as shown in Figure 5J. Furthermore, the
341 addition of these cytokines to ALL cell cultures without stromal cell co-culture demonstrated
342 that IL7 alone increased ALL cell survival, whereas osteopontin and CXCL12 did not
343 (Supplementary Figure 10).

344 Our cell-cell communication analysis revealed that the VCAM1/(ITGA4-ITGB1) axis was
345 exclusively utilized by adipogenic progenitors to interact with ALL cells (Figure 6D). Blocking
346 this interaction in *ex vivo* culture with a VCAM1 blocking antibody led to a decreased viability
347 of leukemic cells in co-culture with adipogenic progenitors, but not with early mesenchymal
348 progenitors or in monoculture (Figure 6E). In contrast, blocking antibodies against integrin
349 beta 1 (ITGB1) or the small peptidomimetic drug BIO-1211, which targets the integrin beta 1
350 binding site, effectively decreased the viability of leukemic cells in co-culture with both
351 stromal populations (Figure 6F & G). This broader effect of ITGB1 blockade is consistent with
352 its involvement in other cell-cell interaction axes with stromal populations, including
353 extracellular matrix proteins as partners, as observed in Figure 6D.

354

355

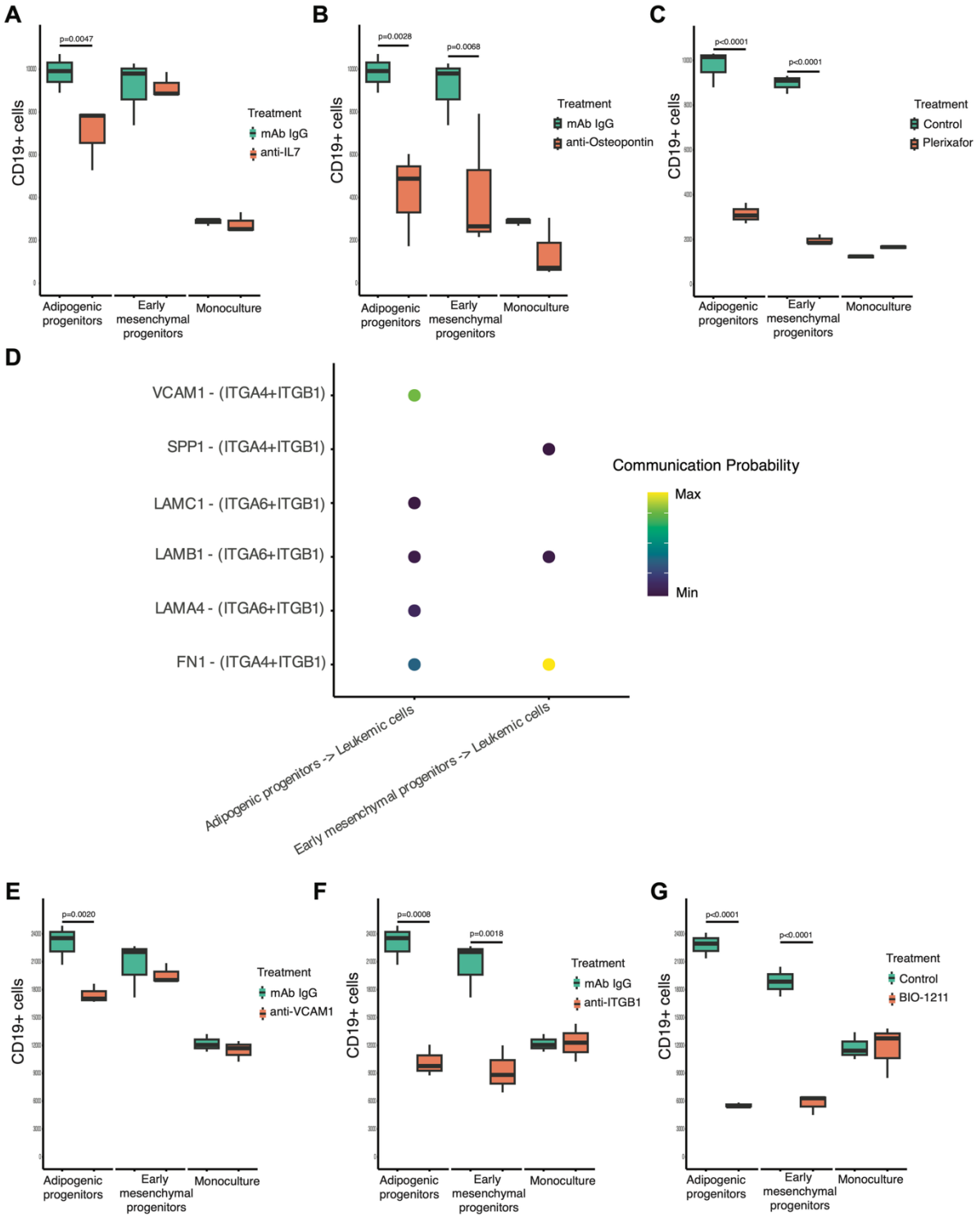

Figure 6. Adipogenic progenitor-specific support of B-ALL cells. Effect of cytokine signaling blockade on ALL cell survival in co-culture with stromal populations. ALL cells were co-cultured with early mesenchymal progenitors, adipogenic progenitors, or cultured alone. Cell survival was assessed after treatment with blocking antibodies against IL7 (A), Osteopontin (B), or the CXCR4 inhibitor Plerixafor (C). D) Ligand-receptor interaction analysis between

363 leukemic cells, adipogenic progenitors and early mesenchymal progenitors. Shown are
364 interactions specifically involving integrin β1 (ITGB1). Dot color reflects interaction probability
365 (from minimum to maximum). E) Effect of VCAM1 blockade on ALL cell viability in co-culture
366 or monoculture. F-G) Effect of blocking integrin beta 1 (ITGB1) using a blocking antibody (F)
367 or the small peptidomimetic drug BIO-1211 (G) on ALL cell viability in co-culture or
368 monoculture.
369

370 ## B-ALL-induced adipogenic bias in stromal cells

371

372 Differential abundance analysis revealed a significant increase in the proportion of adipogenic
373 progenitors in B-ALL patient-derived stromal cells compared to healthy donor-derived cells
374 (Figure 7A & B), suggesting a bias towards the adipogenic lineage in patients with B-ALL. To
375 investigate whether this bias is influenced by the leukemic environment, we assessed the
376 adipogenic differentiation potential of unsorted ex vivo expanded stromal cells derived from
377 B-ALL patients and healthy donors. Our results demonstrated that B-ALL-derived stromal cells
378 exhibited a significantly higher capacity for adipogenic differentiation compared to healthy
379 donor-derived cells (Figure 7C & D). To further explore the underlying mechanisms, we co-
380 cultured healthy donor-derived mesenchymal stromal cells with patient-derived B-ALL cells.
381 We observed that exposure to leukemic cells enhanced MSC differentiation toward the
382 adipogenic lineage (Figure 7E & F), indicating that leukemia-specific factors can directly
383 reprogram stromal cells. Notably, this adipogenic skewing was dependent on cell-cell contact,
384 as evidenced by the lack of enhanced adipogenic differentiation when B-ALL cells and MSCs
385 were cultured in a transwell system (Figure 7G). Collectively, these findings indicate that B-
386 ALL can induce a contact-dependent shift in stromal cell differentiation towards the
387 adipogenic lineage.
388
389

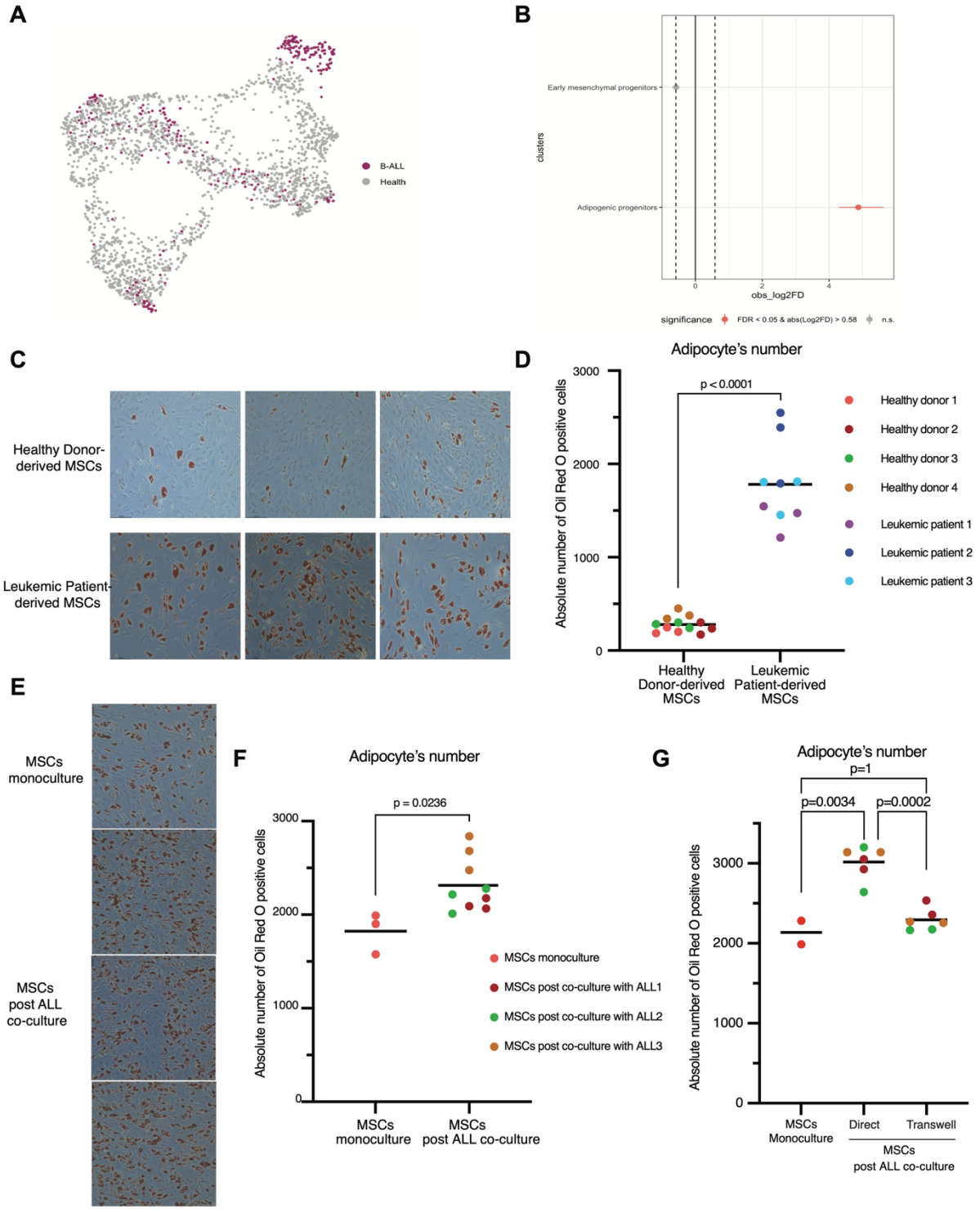

Figure 7. A) UMAP representation of stromal cell clusters from healthy (grey) and ALL patients (violet). B) Point-range plot showing the pairwise proportional difference for each stromal cell cluster (Monte Carlo/permutation test). Red dots indicate statistically significant differences (FDR < 0.05), and vertical dashed lines mark the absolute value of the log2 fold difference (FD) cutoff for significance. C) Representative images of stromal cells derived from three healthy

397 donors (first row) and three leukemic donors (second row) cultured in adipogenic medium for
398 14 days. Oil red O stains lipid droplets (red). D) Quantification of lipid droplet-positive cells
399 per well in a 96-well plate. Data are presented as mean ± standard deviation. Statistical
400 significance was assessed by a two-tailed unpaired Student's t-test. E) Representative images
401 of stromal cells post-monoculture (first column) and post-co-culture with three patient-
402 derived xenografts (second, third, and fourth columns) cultured in adipogenic medium for 14
403 days. Oil red O stains lipid droplets (red). F) Quantification of lipid droplet-positive cells per
404 well in a 96-well plate. Data are presented as mean ± standard deviation. Statistical
405 significance was assessed by a two-tailed unpaired Student's t-test. G) Average number of
406 droplet-positive cells differentiated from MSCs following co-culture with leukemic cells under
407 direct or trans-well conditions (n=2 wells per condition). Data are presented as mean ±
408 standard deviation. Colors depict different patients, as represented in F. Statistical analysis
409 was performed using a linear mixed-effects model with Condition as a fixed effect and Patient
410 as a random effect to account for inter-patient variability. A significant main effect of
411 condition was found (p = 0.00057). Post-hoc pairwise comparisons with Bonferroni correction
412 are shown in the figure.
413
414
415 Stromal niche composition and clinical implications
416
417 The composition of the stromal niche varied between B-ALL patients (Figure 8A). To assess
418 the prevalence of stromal subpopulations in a larger cohort, we performed gene expression
419 deconvolution analysis using CIBERSORTx on a cohort of bone marrow bulk RNA-seq data
420 from 1374 B-ALL patients (Figure 8B), encompassing a range of different molecular subtypes
421 representing the B-ALL genomic landscape (Figure 8C). The abundance of adipogenic
422 progenitors in bone marrow aspirates did not correlate with leukemic burden (Figure 8D).
423 When stratified by sex, no significant differences were observed. A weak but statistically
424 significant negative correlation with age was detected (R= -0.078, p=0.0058), suggesting a
425 slight decrease in abundance with increasing aging (Supplementary Figure 11). Adipogenic
426 progenitor levels varied across molecular subtypes (Figure 8F). Specifically, the ETV6-RUNX1
427 subtype exhibited significantly higher levels of adipogenic progenitors compared to BCR-ABL

(adjusted p = 0.034), BCR-ABL-like (adjusted p = 1.68e-06), CRLF2r (adjusted p = 6.25e-04), Hyperdiploid (adjusted p = 0.003), iAMP21 (adjusted p = 7.80e-05), and PAX5 (adjusted p = 4.93e-04) subtypes. However, despite statistical significance, the visual differences in abundance across subtypes appear modest, suggesting that factors beyond molecular subtype may more strongly influence stromal microenvironment composition. No significant differences in adipogenic progenitor abundance were observed between risk stratification groups (Figure 8E). Importantly, adipogenic progenitors were significantly enriched in patients experiencing relapse, even after correcting for age, sex and molecular subtype, suggesting their involvement in disease progression (Figure 8G).

These findings highlight the heterogeneity of the stromal niche in B-ALL and suggest that adipogenic progenitors may play a crucial role in the leukemic niche.

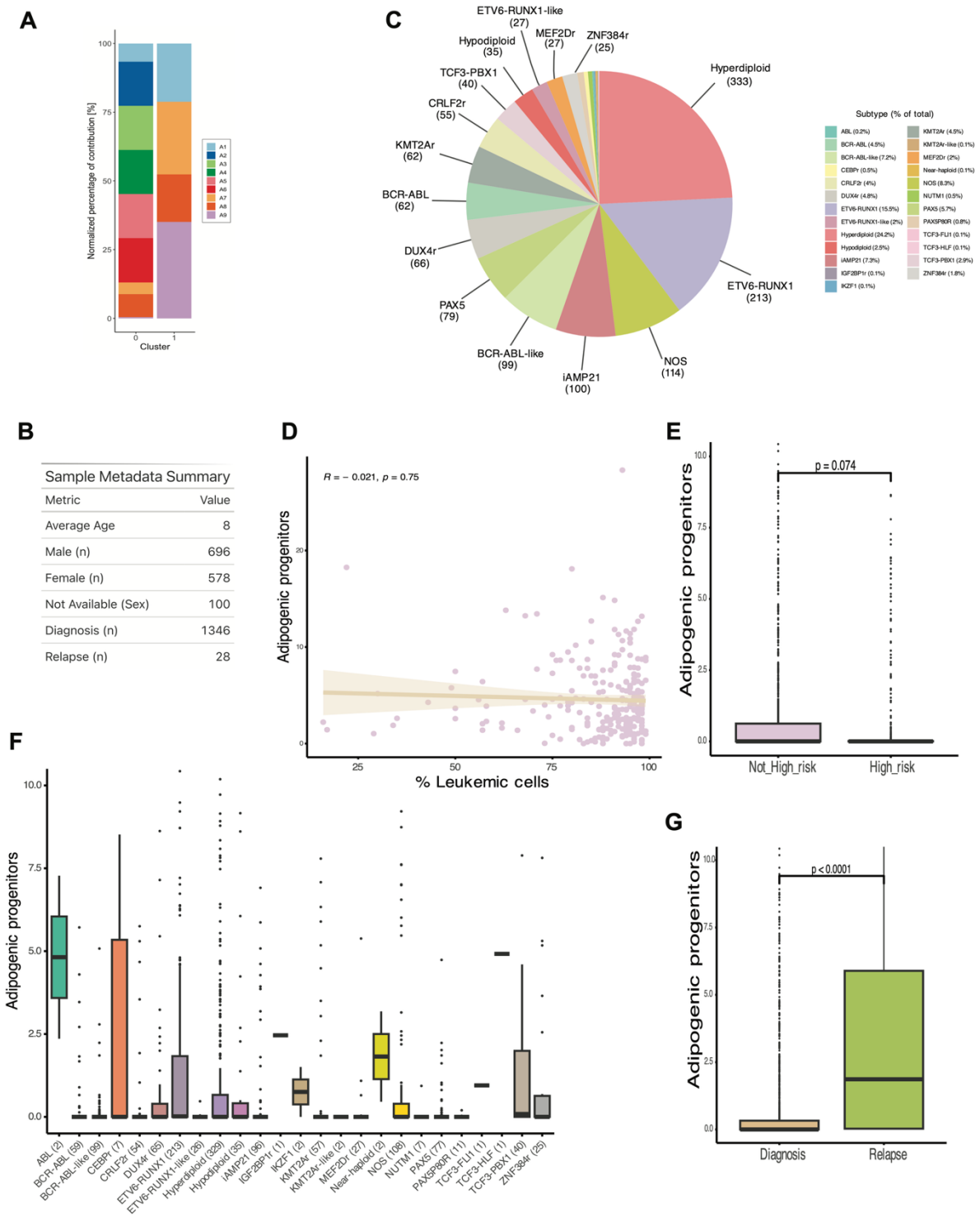

Figure 8. Distinct distribution of stromal cells in B-ALL bone marrow niche. A) Bar plot representing the distribution of stromal cell populations between the different patients analyzed in this study by single-cell RNA sequencing. Early mesenchymal progenitors (cluster 0) and adipogenic progenitors (cluster 1). Each patient sample is represented with a color. B) Sample characteristics of the bulk RNA-seq cohort used for the deconvolution analysis C)

448 Molecular subtype distribution in the cohort. D) Correlation analysis between adipogenic
449 progenitor signature score and the percentage of leukemic cells in bone marrow samples
450 (spearman correlation). E) Comparison of adipogenic progenitor abundance between risk
451 stratification groups. Estimated marginal means (EMMs) were calculated using a linear model
452 adjusting for age and sex (formula: Adipogenic progenitors ~ Risk Stratification + Age + Sex).
453 Pairwise comparisons between risk groups were performed using the emmeans package, and
454 p-values were derived from the contrast of EMMs. F) Analysis of adipogenic progenitors
455 between different molecular subtypes. A Kruskal-Wallis test was used to assess global
456 differences across subtypes ($p = 4.6 \times 10^{-12}$). G) Analysis of the adipogenic progenitors in
457 patients at diagnosis and relapse. Estimated marginal means (EMMs) were derived from a
458 linear model adjusting for age, sex, and molecular subtype (Adipogenic progenitors ~
459 sample_type + Age + Sex + molecular_subtype). Pairwise comparison between sample types
460 was performed using the emmeans package, and the associated p-value was obtained from
461 the contrast of EMMs.
462
463

464 # Discussion

465

466 The bone marrow microenvironment is complex and dynamic and plays a critical role in
467 hematopoiesis and leukemogenesis. Our study provides a comprehensive single-cell
468 transcriptional landscape of the B-ALL niche, revealing a previously unappreciated
469 heterogeneity within the stromal compartment. By identifying distinct early mesenchymal
470 and adipogenic progenitor populations, we have unveiled a more nuanced understanding of
471 the cellular composition of the leukemia-supportive niche.

472

473 Our findings challenge the traditional view of a homogenous stromal population in B-ALL and
474 highlight the importance of considering cellular heterogeneity in the stromal niche. The
475 functional characterization of early mesenchymal and adipogenic progenitors revealed
476 distinct properties, with early mesenchymal progenitors exhibiting a more stem-like
477 phenotype and adipogenic progenitors demonstrating enhanced differentiation capacity.
478 These results suggest that the bone marrow stroma is composed of a continuum of cell states,
479 with early mesenchymal progenitors representing a more primitive population that gives rise
480 to adipogenic and potentially other stromal cell types. These findings are consistent with
481 previous studies describing the heterogeneity of bone marrow MSCs in normal hematopoiesis
482 [14, 16, 17, 31, 32]. However, our study provides new insights into the specific functional roles
483 of these subpopulations in the context of B-ALL.

484

485 The observed difference in proliferation rate between early mesenchymal and adipogenic
486 progenitors suggests that previous studies have overlooked the heterogeneity of the niche
487 due to the selection bias associated with *ex vivo* propagation of MSCs. The more
488 differentiated adipogenic progenitors are less efficient at expanding in culture, leading to an
489 overrepresentation of early mesenchymal progenitors in *ex vivo*-derived stromal populations.
490 This could have contributed to the oversight of the role of adipogenic progenitors in previous
491 studies.

492 Additionally, our study reveals that B-ALL induces a significant shift in stromal cell
493 differentiation towards the adipogenic lineage. We observed an increased proportion of
494 adipogenic progenitors in B-ALL patient-derived stromal cells compared to healthy donor-
495 derived cells, suggesting a leukemia-induced adipogenic bias. This bias was further supported

496 by our finding that B-ALL-derived stromal cells exhibited a higher capacity for adipogenic
497 differentiation. Notably, co-culture experiments demonstrated that ALL-derived factors
498 directly reprogram healthy donor-derived stromal cells, enhancing their differentiation
499 toward the adipogenic lineage, in a contact-dependent manner. These results suggest that
500 leukemic cells actively modulate the bone marrow microenvironment, promoting the
501 generation of adipogenic progenitors as part of their supportive niche, which goes in line with
502 previously published studies demonstrating adipocyte-induced skewing of ALL stroma [33].
503 This adipogenic bias could have profound implications for leukemic progression and therapy
504 resistance, as adipogenic progenitors produce key growth factors and adhesion molecules,
505 such as IL7, SCF, and VCAM1, that support leukemic cell survival.
506
507 Our study reveals that there are distinct stromal niches with which ALL cells can interact. More
508 importantly, our data suggest that ALL cells utilize different modes of interaction with these
509 diverse niche cells. We have previously demonstrated the involvement of N-cadherin in
510 leukemia cell support [8], and now confirm that it is expressed on the early mesenchymal
511 progenitors. In contrast, CXCL12, known to support ALL [30, 34], is primarily expressed by
512 adipogenic progenitors. This complexity underscores the challenges in targeting the niche, as
513 leukemic cells can engage with various environments to survive.
514
515 A key finding of our study is the identification of adipogenic progenitors as a major component
516 of the leukemic niche. These cells resemble previously described marrow adipogenic lineage
517 precursors (MALPs) and Adipo-CXCL12-abundant-reticular cells (Adipo-CAR) in mice [16, 17].
518 Our study provides direct evidence for the involvement of adipogenic progenitor cells in
519 supporting leukemic cell growth and their enrichment at relapse. This observation is in line
520 with previous reports highlighting the role of adipocytes in tumor progression [35].
521 Adipogenic progenitors exhibited high expression of growth factors, such as IL7 and SCF, and
522 adhesion molecules, such as VCAM1, known to support leukemic cell survival, proliferation
523 and therapy resistance [26, 28, 29]. Interestingly, deletion of IL7 in adipogenic progenitors
524 using the Adipoq-Cre transgene mice resulted in severe impairment of B lymphopoiesis [36],
525 suggesting that B cell development relies on adipogenic progenitors. Additionally, deletion of
526 SCF in adipogenic progenitors diminished HSPCs and myeloid progenitors in the bone marrow
527 and led to the development of macrocytic anemia [37], highlighting the crucial involvement

528 of adipogenic progenitors in steady-state hematopoiesis. These findings highlight the broader
529 role of adipogenic progenitors beyond B-ALL and warrant further investigation in other
530 hematological malignancies, such as acute myeloid leukemia.
531
532 The heterogeneity of the stromal niche observed in our patient cohort underscores the
533 complexity of the bone marrow microenvironment in B-ALL and highlights the need for a
534 comprehensive understanding of stromal-leukemic interactions to inform the development
535 of effective niche-targeted therapies. Stratifying patient subgroups based on stromal
536 composition may yield additional prognostic insights and help guide future therapeutic
537 approaches. Clearly, studies involving in-depth characterization and spatial mapping of the
538 leukemic microenvironment across larger patient cohorts are essential to fully elucidate the
539 role of distinct niche components in leukemic progression and resistance to both chemo- and
540 immunotherapy in ALL.
541
542 In conclusion, our study provides novel insights into the cellular complexity of the B-ALL
543 microenvironment and identifies adipogenic progenitors as a key novel component of the B-
544 ALL niche.
545
546 Limitations of the study
547
548 While our study provides novel insights into the B-ALL microenvironment, it is important to
549 acknowledge certain limitations. First, the focus on pediatric patients may limit the
550 generalizability of our findings to adult B-ALL. Second, the sample size of our single-cell RNA
551 sequencing study may not fully capture the variability within the B-ALL patient population.
552 Third, we annotated our pediatric single-cell RNAseq dataset using an atlas derived from total
553 hip arthroplasty samples of adult patients. This might introduce potential caveats due to
554 differences in age, sample source (aspirate versus total tissue) and disease context. Finally,
555 bone marrow biopsies are not routinely performed in children with ALL and, therefore, these
556 analyses rely mostly on bone marrow aspirates. Stroma cell populations that due to their firm
557 attachment to the bone structure are underrepresented in these aspirates, for instance,
558 osteogenic-lineage cells, may add further complexity to the leukemic microenvironment.
559

560 Author contributions

561 **M.N.F.B.** conceptualized the study, conducted bioinformatic analyses, performed ex vivo
562 experiments, interpreted the data, and drafted and prepared the manuscript. **B.K.** conducted
563 the ex vivo assays presented in Figures 3, 4, and 5, and contributed to manuscript writing and
564 preparation. **M.B.** provided critical feedback on the sorting strategy and assisted in
565 manuscript preparation. **O.H.** contributed to supervision and manuscript
566 preparation. **H.J.V.** oversaw the design, interpretation, and analysis of all experiments and
567 contributed to manuscript writing and preparation.

568

569 # Materials and methods

570 **Bone marrow samples**

571 Bone marrow aspirates were obtained from pediatric B-ALL patients in conjunction with
572 routine clinical sampling after obtaining informed consent from parents and/or legal
573 guardians in accordance with institutional review board approval at the Princess Máxima
574 Center (application number PMCLAB2022.305). Bone marrow mononuclear cells (BM-MNCs)
575 were isolated from fresh bone marrow aspirates using density gradient centrifugation and
576 cryopreserved in liquid nitrogen. Healthy donor-derived bone marrow mononuclear cells
577 used in the single-cell RNA-seq analysis were purchased from Stem Cell Technologies
578 (Catalogue 70001). Patient characteristics, including age, gender, genetic risk factors, and
579 disease stage, can be found in Supplementary Table 1.

580

581 **FACs enrichment of stromal, hematopoietic and leukemic cells for scRNAseq**

582 Cryopreserved bone marrow mononuclear cells were thawed and resuspended in RPMI 1640
583 medium containing 5% FBS and 1 mM EDTA. The cell suspension was passed through a 70 µm
584 mesh and stained for 20 minutes at 4 degrees with an antibody cocktail containing CD19-PE
585 (Catalogue 302207, Clone HIB19, 1:100), CD235a-FITC (Catalogue 349103, Clone HI264,
586 1:100), CD45-PE-Cy7 (Catalogue 304015, Clone HI30, 1:100), all from Biolegend. Cells were
587 washed twice with medium followed by 7AAD staining (Catalogue 420404, 1:100) to exclude
588 dead cells before sorting on a Sony SH800S instrument (Sony Biotechnology). Leukemic cells,
589 hematopoietic, and non-hematopoietic cells were sorted in RPMI 1640 medium containing
590 5% FBS. Samples were kept during the whole procedure at 4 °C. Following enrichment, each

591 of the three cell fractions (leukemic, hematopoietic, non-hematopoietic) were resuspended
592 at a concentration of 1000 cells/µL in PBS + 0.04% BSA. Cells were pooled in a 1:1:1 ratio and
593 the cell suspension was subsequently mixed with a cell suspension from another patient with
594 a different gender (multiplexed boy/girl samples). Subsequently, the cell suspension was
595 loaded into the 10x Genomics Chip as described in 'Single-cell RNA library generation'.
596
597 **Single-cell RNA-seq library generation**
598 In total, 20,000 cells were loaded for each (multiplexed) sample onto a 10x Genomics Chip G.
599 We used Chromium Next GEM Single Cell 3' GEM, Library & Gel Bead Kit and followed the
600 protocol as provided by 10x Genomics. Sequencing was performed on Illumina NovaSeq 6000
601 sequencer and parameters were set according to 10x Genomics recommendations. A healthy
602 donor sample was included in the scRNA-seq analysis to provide a baseline for comparison.
603 Only the non-hematopoietic compartment from this sample was sorted and sequenced.
604
605 **Data processing and filtering**
606 Reads from the sequencing were aligned to the human reference genome (GRCh38) using Cell
607 Ranger v7.1.0. Samples were demultiplexed using souporcell based on Single Nucleotide
608 Polymorphisms (SNPs) identified within the reads. Patient identities were assigned based on
609 specific sex chromosome genes. Further analysis was performed using R v4.0.2
610 (https://www.r-project.org/) including several packages which are mentioned in the
611 according section. As an initial step, we filtered out low-quality cells. Cells with less than 200
612 expressed features were removed. Additionally, cells with greater than 10% of reads mapping
613 to mitochondrial genes were excluded. Doublets/multiplets, which can arise during library
614 preparation, were identified and removed using the scDblFinder package with default
615 parameters [38].
616
617 **Data integration**
618 All patient scRNAseq datasets were merged into one Seurat object after prefiltering (see
619 section: "Data processing and filtering"). Based on this object, the data was normalized using
620 the SCTransform function from Seurat with default parameters. Principal component analysis
621 (PCA) was performed using the RunPCA function from Seurat, with the number of principal
622 components (npcs) set to 30, a value determined empirically to capture the major sources of

623 variation in the data. The IntegrateLayers function was run with the RPCA integration method
624 and default settings to integrate the data across different patients and account for batch
625 effects.
626
627 **Annotation**
628 Cluster annotation for the full integration of all samples was performed at a low-resolution to
629 identify major cell types. Cell types were annotated based on information from literature,
630 functional information from gene sets based on the marker genes of a cluster and unbiased
631 cell type recognition using the Human Primary Cell Atlas and bone marrow scRNAseq
632 references [14, 15] in SingleR with default parameters [39]. The cell type annotation of the
633 stromal cluster relied primarily on the dataset by Bandyopadhyay et al. as a reference in
634 SingleR using default parameters. Unsupervised clustering of the stromal cluster using the
635 FindClusters function in Seurat identified 5 subclusters. However, the biological relevance and
636 distinct cell identities of these subclusters could not be elucidated based on their top markers.
637 Furthermore, the transcriptome of 4 of these subclusters exhibited greater similarity to each
638 other compared to the fifth cluster. To further investigate the stromal cell populations, single-
639 cell RNA-seq data from the manuscript of Bandyopadhyay et al, Cell 2024 [14], was
640 downloaded from NCBI Gene Expression Omnibus (GSE253355) and loaded into Seurat. This
641 comparative analysis predominantly identified two stromal populations: early mesenchymal
642 progenitors (fibro-MSCs) and adipogenic progenitors (adipo-MSCs).
643
644 **Marker gene identification**
645 Marker genes per cluster were calculated by the Seurat function FindAllMarkers, using the
646 method "Model-based Analysis of Single-cell Transcriptomics" (MAST) with a log fold change
647 threshold of 0.3 and min-pct set to 0.3. Enriched gene sets per set of marker genes were
648 analyzed as described in the Gene Set Enrichment Analysis section.
649
650 **Gene set enrichment analysis (GSEA)**
651 The gprofiler2 package was used to perform GSEA based on marker genes and differentially
652 expressed genes [40]. The gost function was run with default settings. Ribosomal genes were
653 excluded from the gene lists beforehand to focus on biologically relevant processes and only
654 gene lists with more than 5 remaining genes sorted by adjusted p value were tested. Before

655 plotting, the identified gene sets were filtered for terms with less than 1000 genes to exclude
656 overly broad terms. Only terms from GO, Reactome and KEGG were plotted.
657
658 **Signal pathway activity**
659 To investigate signaling pathway activity across stromal cell populations, we utilized the R
660 package PROGENy [41]. The integrated Seurat object was used to annotate stromal
661 subpopulations and compute pathway activity scores using the top 500 genes relevant for
662 human signaling pathways. PROGENy scores were added to the Seurat object as a new assay
663 and scaled using Seurat's ScaleData function. Pathway scores were extracted and aggregated
664 by cell type to compute average activity levels per population. Visualization of global and
665 selected pathway activities was performed using heatmaps (pheatmap package), displaying
666 the average pathway activity per cell type.
667
668 **Transcription factor activity inference using SCENIC**
669 To infer transcription factor (TF) activity across stromal populations in B-ALL, we applied the
670 SCENIC (Single-Cell rEgulatory Network Inference and Clustering) pipeline [18].. Raw gene
671 expression counts were extracted from an integrated Seurat object containing stromal cells.
672 SCENIC was executed in R using the GENIE3, RcisTarget, and AUCell packages with human
673 motif annotations and cisTarget databases (hg19) for regulatory network inference. Regulon
674 activity was summarized per stromal cluster and visualized using heatmaps to identify cell
675 type-specific TF programs.
676
677 **Differentiation state prediction**
678 To infer the differentiation potential of stromal cells, we employed CytoTRACE v0.3.3, a
679 computational tool that estimates developmental states based on gene expression profiles
680 and transcriptional entropy [42]. We began by extracting the raw count matrix from the RNA
681 assay of the Seurat object. This count matrix was converted into a data frame suitable for
682 input into the CytoTRACE algorithm. CytoTRACE was then run using default parameters,
683 returning a differentiation score for each cell, where higher scores reflect a more progenitor-
684 like state and lower scores indicate greater differentiation. The CytoTRACE scores were
685 subsequently added to the Seurat object as metadata. Ridge plots were created to
686 characterize the density of differentiation states across cell types.

687

688 **Cell-cell communication analysis**

689 The CellChat algorithm was applied to perform an unbiased ligand-receptor interaction
690 analysis [43]. CellChat's human ligand-receptor database was employed to infer potential cell-
691 cell interactions. Overexpressed genes and interactions were identified, followed by
692 projection onto a human protein-protein interaction network. Communication probabilities
693 were computed using a tri-mean method, and signaling pathways were aggregated and
694 filtered to include interactions supported by at least 10 cells per group. Network centrality
695 metrics were calculated, and interaction patterns were visualized via circle plots and bubble
696 plots (targeted to key populations such as adipogenic and early mesenchymal progenitors,
697 and leukemic cells).

698 A leukemic cell interaction score was calculated per cell cluster as the average expression of
699 signaling factors (cytokines, integrins, extracellular membrane components) that were
700 inferred to interact with leukemic cells based on the CellChat inferred interactions, using a
701 curated gene set of 45 nourishing ligands (e.g., CXCL12, FN1, VEGFA, GDF15). Module scores
702 were calculated per cell, and statistical differences across non-leukemic cell types were
703 evaluated using Kruskal-Wallis and post-hoc Bonferroni-adjusted Wilcoxon tests.

704 To identify dominant modes of outgoing intercellular communication, non-negative matrix
705 factorization (NMF) was applied to the signaling networks. The optimal number of outgoing
706 signaling patterns was determined using the selectK() function, which evaluates cophenetic
707 and silhouette coefficients; both metrics indicated an elbow at k = 5, suggesting five distinct
708 communication programs. These five communication patterns represent core signaling
709 strategies employed by different cell types across the microenvironment. Each pattern groups
710 cell populations that exhibit similar outgoing signaling behaviors, highlighting functional
711 convergence or specialization.

712

713 **Inference of copy number variation.**

714 To distinguish leukemic cells from non-malignant populations in pediatric B-ALL samples, we
715 performed copy number alteration (CNA) analysis on individual patients using the SCEVAN
716 (Single-Cell Evolutionary Variational Autoencoder for CNAs) R package [44]. For each patient,
717 we extracted single-cell gene expression data from an integrated Seurat object. To define a
718 set of reference "normal" cells for CNA inference, clusters corresponding to T cells and

719 monocytes were identified based on expression of canonical markers such as CD3G, CD8A,
720 CD14, and FCGR3A, using DotPlot() visualization. Cells from clusters expressing these markers
721 were selected as the normal reference population. Gene expression matrices were extracted
722 from the RNA assay for each sample and converted to matrix format for input into the
723 pipelineCNA() function from the SCEVAN package. SCEVAN output classified cells based on
724 inferred CNA profiles into likely malignant or normal categories.
725
726 **Spatial transcriptomic analysis.**

727 We analyzed a publicly available spatial transcriptomics dataset generated using the Xenium
728 In Situ platform (10x Genomics) from a formalin-fixed paraffin-embedded (FFPE) trephine
729 bone marrow biopsy sample obtained from a patient diagnosed with B-cell acute
730 lymphoblastic leukemia (B-ALL) [25]. Patient metadata, including age, sex, and molecular
731 subtype, were not provided with the dataset. The dataset consisted of a total
732 of 225,906 spatially resolved cells. The median number of transcripts per cell was 27, and a
733 total of 6,933,297 high-quality decoded transcripts were detected across the tissue section.
734 The total imaged region area was 26,288,545.2 μm^2. Gene expression profiling was
735 performed using a panel of 477 RNA targets, which included 377 predesigned genes from the
736 standard Xenium Human Multi-Tissue Panel and 100 custom-selected genes relevant to bone
737 marrow.

738 Cell segmentation was performed using the Xenium onboard pipeline. Nuclear boundaries
739 were identified based on DAPI staining, and a heuristic expansion was applied to approximate
740 full cell boundaries, enabling transcript assignment to individual cells. Xenium data was
741 analyzed using the Seurat (v5) R packages. Xenium raw data were imported
742 with LoadXenium() and filtered to retain cells with >10 UMIs and >3 detected genes. Quality
743 control metrics were visualized using violin plots. Selected regions of interest were cropped
744 for high-resolution spatial inspection using the Crop() function. Normalization was performed
745 using SCTransform. Principal component analysis (PCA), uniform manifold approximation and
746 projection (UMAP), and shared nearest neighbor-based clustering were used for
747 dimensionality reduction and cell clustering
748 (RunPCA(), RunUMAP(), FindNeighbors(), FindClusters()), with clustering resolution set to 0.2

749 for the full dataset. Marker genes for each cluster were identified via differential expression
750 analysis using the MAST test (FindAllMarkers()), applying a threshold of log2FC > 0.1 and
751 adjusted p-value < 0.05. To identify and map specialized cellular microenvironments, spatial
752 niches were inferred using the BuildNiche()function from Seurat with standard settings, which
753 detects spatially enriched co-localized cell populations. For spatial visualization, annotated
754 cell identities were exported and visualized using Xenium Explorer 3.0.

755 **Generation of single-cell reference matrix**

756 A single-cell RNA-seq reference was constructed using our integrated dataset encompassing
757 all cellular populations within the B-ALL niche. A reference expression matrix was generated
758 by extracting raw count data from the RNA assay using GetAssayData() with the "counts"
759 layer. The resulting matrix was converted to a data.frame and matched with corresponding
760 cell-type annotations. The column names of the expression matrix were relabeled with their
761 respective "Annotation_L2" identities to ensure compatibility with CIBERSORT, which
762 requires labeled expression profiles as input. The final reference matrix was saved as a tab-
763 delimited text file (.txt) for use in downstream deconvolution of bulk RNA-seq data.

764 **Cell type deconvolution Analysis in Bulk RNA-seq Data**

765 Bulk RNA-seq data generated for routine diagnostics were obtained from the Princess Máxima
766 Center Biobank (application number PMCLAB2021.258), containing a cohort of 245 B-ALL
767 bone marrow patient samples. Furthermore, we obtain a publicly available dataset
768 downloaded from the St. Jude Cloud Platform via DNAnexus [45]. For RNA-seq deconvolution,
769 we employed CIBERSORTx with the Impute Cell Fractions job type, with batch correction S-
770 mode, in absolute mode and 100 permutations. Clinical metadata including age, sex,
771 molecular subtype, and sample type (diagnosis vs. relapse) were imported into R for further
772 analysis. Samples were grouped into risk categories (High vs. Not High Risk) based on the
773 molecular subtype according to criteria described in the literature [46], and annotated
774 accordingly. Samples were categorized as High Risk if they harbored one of the following
775 subtypes: BCR-ABL, BCR-ABL-like, KMT2A rearranged (KMT2Ar), hypodiploid, near-haploid,
776 MEF2D rearranged (MEF2Dr), MYC, iAMP21, TCF3-HLF, or ABL-class fusions. Samples were
777 categorized as Not High Risk if they exhibited one of the following subtypes: ETV6-RUNX1,
778 ETV6-RUNX1-like, hyperdiploid, TCF3-PBX1, DUX4 rearranged (DUX4r), CRLF2 rearranged

779 (CRLF2r), CEBP rearranged (CEBPr), KMT2A-like, ZNF384-like (ZNF384r-like), PAX5, ZNF384
780 rearranged (ZNF384r), IGF2BP1 rearranged (IGF2BP1r), IKZF1, or other. Outlier detection was
781 performed on the adipogenic progenitor scores using visual inspection of histograms and
782 Grubbs' test. One extreme outlier (value >300) was identified and excluded from downstream
783 analyses.
784
785 **Stromal populations cell sorting**
786 MSC subtypes were isolated from BM-MNCs using fluorescence-activated cell sorting (FACS)
787 on a Sony SH800S instrument (Sony Biotechnology) based on surface marker expression
788 identified from the single-cell RNA sequencing data. In addition to the analysis of well-known
789 stromal CD markers, we performed an unbiased approach using the sc2marker package with
790 default settings [47].
791 To exclude hematopoietic and leukemic cells, we used a dump gate strategy at 421 nm
792 emission composed of CD19-BV421 (Catalogue 302233, clone HIB19, 1:100), CD22-BV421
793 (Catalogue 302523, clone HIB22, 1:100), CD45-BV421 (Catalogue 304031, clone HI30, 1:100),
794 CD235a-BV421 (Catalogue 349131, clone, HI264 1:100). Live/dead exclusion was performed
795 using Zombie green (Catalogue 423111, 1:100). Adipogenic progenitors were sorted as
796 positive for CD106-PE (Catalogue 305805, clone STA, 1:100) and Cadherin 11-APC (Catalogue
797 368705, clone 16G5, 1:100), while early mesenchymal progenitors were negative for these
798 markers and positive for CD81-PE-Cy7 (Catalogue 349511, clone 5A6, 1:100) and CD90-AF700
799 (Catalogue 328119, clone 5E10, 1:100). Stromal populations were sorted in MSC medium
800 (DMEM-low glucose supplemented with 10% FBS, 1% Primocin solution and 1 ng/mL bFGF).
801
802 **scRNA seq analysis of early mesenchymal progenitors and adipogenic progenitors**
803 Sorted MSC subtypes were cultured in MSC medium (DMEM-low glucose supplemented with
804 10% FBS, 1% Primocin solution and 1 ng/mL bFGF) and incubated at 37 °C with 5% CO2. Cells
805 were expanded to passage 3 and scRNAseq analysis was performed as described in 'Single-
806 cell RNA library generation'.
807
808 **Projection of sorted stromal populations into the unsorted stromal scRNAseq dataset**
809 The two stromal populations were isolated via FACS from leukemic donor samples and
810 sequenced independently. To control for sampling bias, each sorted population was

811 downsampled to 2,300 cells. Each dataset was normalized using the SCTransform function,
812 regressing out mitochondrial content. Following normalization, the datasets were merged
813 and dimensionality reduction was performed using PCA (30 components), followed by UMAP.
814 The merged dataset of sorted stromal cells was projected onto the UMAP embedding of the
815 reference stromal dataset using the RunKNNMap function from the SCP package. The
816 projection utilized 3,000 integration features identified via SelectIntegrationFeatures, and
817 both query and reference datasets used the SCT assay. Following projection, cells from the
818 sorted populations were classified according to the nearest neighbors in the reference using
819 RunKNNPredict. Cells were assigned to predicted stromal subtypes with a low-frequency filter
820 set at 20 cells per type. To quantify enrichment of predicted stromal subtypes within each
821 sorted population, classification outcomes were tabulated and expressed as proportions. A
822 contingency table comparing the frequencies of adipogenic versus early mesenchymal
823 progenitors across the two sorted populations was constructed. A chi-square test of
824 independence was used to evaluate differences in predicted subtype distributions between
825 sorted populations. Proportional distributions of predicted stromal subtypes were visualized
826 using stacked bar plots in ggplot2, with custom color palettes for clarity.
827
828 **Flow cytometry analysis of sorted early mesenchymal progenitors and adipogenic**
829 **progenitors**
830 Sorted MSC subtypes were cultured in MSC medium (DMEM-low glucose supplemented with
831 10% FBS, 1% Primocin solution and 1 ng/mL bFGF) and incubated at 37 °C with 5% CO2. Cells
832 were expanded to passage 3, trypsinized and prepared for flow cytometry analysis. The cell
833 suspension was stained with Viakrome 808 (Catalogue #C36628, 1:100, Beckman Coulter) for
834 15 minutes at 4 degrees to exclude dead cells. After staining, 1 mL of MSC medium was added
835 to the suspension, which was then centrifuged. The supernatant was discarded, and the cell
836 pellet was resuspended in a single marker antibody solution. All antibodies were obtained
837 from Biolegend. Following antibody staining, cells were washed with PBS containing 1% FBS,
838 centrifuged and the supernatant was discarded. The final cell pellet was resuspended in 100
839 microliters of PBS containing 1% FBS fow flow cytometry analysis on a Cytoflex LX instrument
840 (Beckman Coulter). Data were analyzed using FlowJo software (BD Biosciences).
841
842 **Colony-forming unit fibroblast (CFU-F) assays**

843 Sorted cells were seeded in 6-well plates at a density of 475 cells per well (50 cells/cm2)
844 containing culture medium (DMEM-low glucose supplemented with 10% FBS, 1%
845 Penicillin/Streptomycin solution and 1 ng/mL bFGF) and incubated at 37 °C with 5% CO2.
846 Medium was changed every 3–4 days. At day 10, cells were fixed with methanol and stained
847 with 0,5% crystal violet staining solution. Adherent colonies with more than 50 cells were
848 quantified.
849
850 **Multipotency assays**
851 Adipogenic and osteogenic differentiation assays were performed in cells at passage three to
852 five. For adipogenic differentiation, cells were seeded at a density of 21,000 cells/ cm2 and
853 cultured in DMEM-low glucose (Gibco, Catalogue 21885-025) supplemented with 10% FBS,
854 1% Penicillin/Streptomycin, 0.5 µM isobutylmethylxanthine (Sigma, I5879), 60 µM
855 indomethacin (Sigma, 17378), 5 µg/mL insulin (Sigma, I9278) and 1 µM dexamethasone
856 (Sigma, D2915) for 15 days (medium was changed every 3-4 days). To measure adipogenic
857 differentiation, cells were fixed with 4% PFA and stained using 0.5% Oil Red O (Sigma, 00625)
858 in isopropyl alcohol diluted with distilled water in 3:2 ratio and the lipid-filled cells across the
859 whole well of a 96-well plate were counted. Images of stained cells from corresponding
860 samples in 12-well plates were captured for visualization.
861 For osteogenic differentiation, cells were seeded at a density of 3000 cells/ cm2 in osteogenic
862 medium for 15 days (medium was changed every 3-4 days). The osteogenic differentiation
863 medium contained DMEM supplemented with 10% FBS, 1% Penicillin/Streptomycin, 1%
864 glutamine, 50 µg/mL L-ascorbate acid (Sigma, A8960), 10 mM β-glycerophosphate (Sigma,
865 G6376) and 100 nM dexamethasone. Osteogenic differentiation was verified by alizarin red S
866 staining (Sigma, A5533) by visualization of mineralized deposits.
867
868 **Leukemic cell viability in co-culture with stromal populations**
869 Early mesenchymal progenitors and adipogenic progenitors between passages 5-7 were
870 seeded at a cell density of 15,000 cells/cm2 in 96 well plate in MSC medium and incubated at
871 37 °C with 5% CO2. The next day, 200,000 patient-derived bone marrow mononuclear cells
872 and sorted MSC subtypes were co-cultured in SFEM medium containing 1%
873 Penicillin/Streptomycin solution and incubated at 37 °C with 5% CO2. After 7 days, all cells
874 per well were harvested by aspirating the supernatant and trypsinizing attached cells using

875 TrypLE Express (Gibco, 12605). Both cell suspensions were combined, per well. After washing
876 the cells with PBS, FBS 5%, cells were stained with CD19-BV421 (Biolegend, Catalogue 302233,
877 clone HIB19, 1:100) and Zombie NIR (Biolegend, Catalogue 423106, 1:200) for live/dead
878 exclusion.
879 Cell viability was assessed using a flow cytometry Cytoflex S (Beckman Coulter), recording all
880 events with a fixed volume of 80 microliters per well.
881
882 **Evaluation of small molecules and blocking antibodies in co-culture of B-ALL cells with**
883 **stromal populations.**
884 Early mesenchymal progenitors and adipogenic progenitors between passages 5-7 were
885 seeded at a cell density of 15,000 cells/cm2 in 96 well plate in MSC medium and incubated at
886 37 °C with 5% CO2. The next day, 200,000 patient-derived bone marrow mononuclear cells
887 were added per well in 200ul SFEM containing 1% Penicillin/Streptomycin. Where indicated,
888 cultures were treated with varying dexamethasone (Sigma, D4902) concentrations (1 nM, 3
889 nM, 5 nM, 10 nM, 30 nM, 50 nM, 100nM), mouse IgG1 kappa Isotype control (1 ug/mL,
890 MedChemExpress, Catalogue HY-P99977), anti-mouse/human IL-7 (1 ug/mL, BioCell, Clone
891 M25, Catalogue BE0048), Plerixafor (1 nM, MedChemExpress, Catalogue HY-10046), anti-
892 Osteopontin (1 ug/mL, BE0382, BioCell), BIO-1211 (50uM, MedChemExpress, Catalogue HY-
893 14126), anti-hVCAM1 mouse monoclonal IgG (2 ug/mL, R&D Systems, Clone BBIG-V1,
894 Catalogue BBA5), and anti-Integrin Beta1 (2 ug/mL, Merk, Clone AIIB2, Catalogue MABT409).
895 After 7 days of incubation, all cells per well were harvested by aspirating the supernatant and
896 trypsinizing attached cells using TrypLE Express (Gibco, 12605). Both cell suspensions were
897 combined, per well. After washing the cells with PBS, FBS 5%, cells were stained with CD19-
898 PE (Biolegend, Catalogue 302208, Clone HIB19, 1:100) and Zombie Violet Fixable Viablity Kit
899 (BioLegend, Catalogue 423113/423114, 1:100) for live/dead exclusion. The flow cytometry
900 analysis on a Cytoflex LS instrument (Beckman Coulter) was used to measure absolute number
901 of viable CD19+ leukemic cells per well. Data was analyzed with FlowJo software (BD
902 Biosciences).
903
904 **Isolation of pediatric bone marrow stromal cells from healthy and leukemic patients.**
905 Healthy donor-derived stromal cells were isolated from surplus iliac crest bone chip material
906 harvested from pediatric patients undergoing alveolar bone graft surgery. All human samples

907 were obtained with the approval of the Erasmus MC, University Medical Center Medical
908 Research Ethics Committee (MEC-2014-16). Iliac crest bone chips were washed with
909 expansion medium composed of Minimum Essential Medium (MEM)-α (containing
910 nucleosides) supplemented with heat inactivated 10% v/v fetal bovine serum (FBS) (both
911 Thermo Fisher Scientific, Waltham, MA, USA), 1.5 µg/ml fungizone (Gibco), 50 µg/ml
912 gentamicin (Gibco), 25 µg/ml L-ascorbic acid 2-phosphate (Sigma-Aldrich, St. Louis, MO, USA),
913 and 1 ng/ml fibroblast growth factor-2 (Instruchemie, Delfzijl, The Netherlands), and the
914 resulting cell suspension was seeded in T75 flasks. Cells were washed twice with phosphate
915 buffered saline (Thermo Fisher Scientific) supplemented with 2% v/v heat inactivated FBS 24
916 hours following seeding to remove non-adherent cells. Stromal cells were cultured at 37°C
917 and 5% carbon dioxide under humidified conditions, with expansion medium refreshed every
918 3–4 days. A similar approach was used to isolate stromal cells from bone marrow aspirates
919 from B-ALL patients (application number PMCLAB2022.305). 24 hours after seeding, the non-
920 attached cells were removed and adherent cells were cultured at 37°C and 5% carbon dioxide
921 under humidified conditions, with expansion medium refreshed every 3–4 days.
922 Stromal cells were sub-cultured upon reaching 80–90% confluency using 0.25% w/v trypsin-
923 EDTA (Thermo Fisher Scientific) and reseeded at a cell density of 2,300 cells/cm2.
924 Adipogenic differentiation was performed with leukemic and healthy donor-derived stromal
925 cells at passage 5 as described in the section 'Multipotency assays'.
926
927 **Analysis of adipogenic differentiation skewing by leukemic cells**
928 Healthy donor -derived stromal cells were co-cultured with patient-derived xenografts in
929 SFEM medium containing 1% Penicillin/Streptomycin solution and incubated at 37 °C with 5%
930 CO2. After 24 hours, leukemic cells were removed by aspirating the supernatant. After
931 washing the cells with PBS, FBS 5%, adipogenic differentiation was induced and quantified as
932 described in the section 'Multipotency assays'.
933 In the same manner, 12-well hanging cell culture inserts, PET membrane, with a pore size of
934 0.4 µm (cellQART, 9310402) were used for the transwell assay. Three days later, leukemic
935 cells were removed, and the remaining cells were cultured in adipogenic differentiation media
936 for 12 days to match 15 days of adipogenic differentiation period. Five pictures per well were
937 taken at 2X magnification and based on that the average number of lipid containing cells/well
938 was calculated.

939

940 **Multiplex cytokine analysis**

941 Harvested supernatant (25 µL) was used for cytokine quantification using a bead-based
942 immunoassay according to the manufacturer's instructions (LEGENDplex, BioLegend,
943 Catalogue 741362 and 740611). Specific antibody coated beads were incubated with
944 supernatant from each condition, in triplicate, forming an analyte-antibody complex. After
945 washing, a biotinylated detection antibody cocktail was added which bound to the specific
946 analyte-antibody complexes. Streptavidin-phycoerythrin was subsequently added which
947 bound to the biotinylated detection antibodies, providing fluorescent signal intensities in
948 proportion to the bound analyte amount. Fluorescent signals were measured using Cytoflex
949 LX and analysed using LEGENDplex data analysis software where concentrations of each
950 analyte were determined using a standard curve generated from the same assay.

951

952 **Statistical Analysis**

953 Unless otherwise stated, statistical significance was assessed by a two-tailed Student's t-test
954 for comparison between two groups or two-way ANOVA with Bonferroni's multiple
955 comparison for comparisons among multiple groups. A p value < 0.05 was considered
956 statistically significant. Statistical analyses were performed using GraphPad Prism 9.0.1 and
957 R. GSEA is performed with the hypergeometric test for overrepresentation (one-sided),
958 followed by multiple comparison correction using the Benjamini-Hochberg method. The
959 individual method of correction for specific R packages are described in the corresponding
960 publications.

961

962 **Data availability**

963 The single-cell RNA sequencing data generated in this study have been deposited in Zenodo
964 at 10.5281/zenodo.13755294. All other relevant data supporting the key findings of this study
965 are available within the article and its Supplementary Information files or from the
966 corresponding author upon request.

967

968 **Code availability**

969 Custom scripts are available at:
970 https://github.com/mauriferrao/ALL_Stromal_Microenvironment.git

Any additional information required to reanalyze the data reported in this paper is available from the corresponding author upon request.

Acknowledgements

We would like to thank the single cell sequencing facility, the flow cytometry facility at the Princess Máxima Center, Polina Derevianko, Daniel Mata Casimiro, Anita van Oort and Elizabeth Schweighart for their assistance.

Funding

This work has been supported by Horizon Europe's Marie Sklodowska – Curie Actions co-fund project number 101081481 (Butterfly), KiKa project number 329, ERC (grant no. 101114895) and Landsteiner Foundation for Blood Research (grant no. 2305F).

Declaration of interests

The authors declare no competing interests.

References

1. Ding, L. and S.J. Morrison, *Haematopoietic stem cells and early lymphoid progenitors occupy distinct bone marrow niches.* Nature, 2013. **495**(7440): p. 231-5.
2. Mendez-Ferrer, S., et al., *Mesenchymal and haematopoietic stem cells form a unique bone marrow niche.* Nature, 2010. **466**(7308): p. 829-34.
3. Bianco, P. and P.G. Robey, *Skeletal stem cells.* Development, 2015. **142**(6): p. 1023-7.
4. Kunisaki, Y., et al., *Arteriolar niches maintain haematopoietic stem cell quiescence.* Nature, 2013. **502**(7473): p. 637-43.
5. Greenbaum, A., et al., *CXCL12 in early mesenchymal progenitors is required for haematopoietic stem-cell maintenance.* Nature, 2013. **495**(7440): p. 227-30.
6. Sugiyama, T., et al., *Maintenance of the hematopoietic stem cell pool by CXCL12-CXCR4 chemokine signaling in bone marrow stromal cell niches.* Immunity, 2006. **25**(6): p. 977-88.
7. Duan, C.W., et al., *Leukemia propagating cells rebuild an evolving niche in response to therapy.* Cancer Cell, 2014. **25**(6): p. 778-93.
8. Pal, D., et al., *hiPSC-derived bone marrow milieu identifies a clinically actionable driver of niche-mediated treatment resistance in leukemia.* Cell Rep Med, 2022. **3**(8): p. 100717.

1007 9. Park, C.S., et al., *Stromal-induced epithelial-mesenchymal transition induces*
1008 *targetable drug resistance in acute lymphoblastic leukemia.* Cell Rep, 2023. **42**(7): p.
1009 112804.
1010 10. Witkowski, M.T., et al., *Extensive Remodeling of the Immune Microenvironment in B*
1011 *Cell Acute Lymphoblastic Leukemia.* Cancer Cell, 2020. **37**(6): p. 867-882 e12.
1012 11. Zyla, J., et al., *Evaluation of zero counts to better understand the discrepancies*
1013 *between bulk and single-cell RNA-Seq platforms.* Comput Struct Biotechnol J, 2023.
1014 **21**: p. 4663-4674.
1015 12. Sotillo, E., et al., *Convergence of Acquired Mutations and Alternative Splicing of CD19*
1016 *Enables Resistance to CART-19 Immunotherapy.* Cancer Discov, 2015. **5**(12): p. 1282-
1017 95.
1018 13. Witkowski, M.T., et al., *NUDT21 limits CD19 levels through alternative mRNA*
1019 *polyadenylation in B cell acute lymphoblastic leukemia.* Nat Immunol, 2022. **23**(10):
1020 p. 1424-1432.
1021 14. Bandyopadhyay, S., et al., *Mapping the cellular biogeography of human bone*
1022 *marrow niches using single-cell transcriptomics and proteomic imaging.* Cell, 2024.
1023 **187**(12): p. 3120-3140 e29.
1024 15. Stuart, T., et al., *Comprehensive Integration of Single-Cell Data.* Cell, 2019. **177**(7): p.
1025 1888-1902 e21.
1026 16. Zhong, L., et al., *Single cell transcriptomics identifies a unique adipose lineage cell*
1027 *population that regulates bone marrow environment.* Elife, 2020. **9**.
1028 17. Tikhonova, A.N., et al., *The bone marrow microenvironment at single-cell resolution.*
1029 Nature, 2019. **569**(7755): p. 222-228.
1030 18. Aibar, S., et al., *SCENIC: single-cell regulatory network inference and clustering.* Nat
1031 Methods, 2017. **14**(11): p. 1083-1086.
1032 19. Gao, H., et al., *Early B cell factor 1 regulates adipocyte morphology and lipolysis in*
1033 *white adipose tissue.* Cell Metab, 2014. **19**(6): p. 981-92.
1034 20. Ambele, M.A., et al., *Adipogenesis: A Complex Interplay of Multiple Molecular*
1035 *Determinants and Pathways.* Int J Mol Sci, 2020. **21**(12).
1036 21. He, J., et al., *Dissecting human embryonic skeletal stem cell ontogeny by single-cell*
1037 *transcriptomic and functional analyses.* Cell Res, 2021. **31**(7): p. 742-757.
1038 22. Aouadi, M., et al., *p38MAP Kinase activity is required for human primary adipocyte*
1039 *differentiation.* FEBS Lett, 2007. **581**(29): p. 5591-6.
1040 23. Bost, F., et al., *The extracellular signal-regulated kinase isoform ERK1 is specifically*
1041 *required for in vitro and in vivo adipogenesis.* Diabetes, 2005. **54**(2): p. 402-11.
1042 24. Richard, A.J. and J.M. Stephens, *The role of JAK-STAT signaling in adipose tissue*
1043 *function.* Biochim Biophys Acta, 2014. **1842**(3): p. 431-9.
1044 25. *Acute Lymphoid Leukemia Bone Marrow, In Situ Gene Expression, Xenium Onboard*
1045 *Analysis by Xenium Analyzer*. 2024, 10x Genomics.
1046 26. Mendez-Ferrer, S., et al., *Bone marrow niches in haematological malignancies.* Nat
1047 Rev Cancer, 2020. **20**(5): p. 285-298.
1048 27. Hughes, A.M., et al., *The Bone Marrow Microenvironment in B-Cell Development and*
1049 *Malignancy.* Cancers (Basel), 2022. **14**(9).
1050 28. Pinho, S., et al., *PDGFRalpha and CD51 mark human nestin+ sphere-forming*
1051 *mesenchymal stem cells capable of hematopoietic progenitor cell expansion.* J Exp
1052 Med, 2013. **210**(7): p. 1351-67.

1053 29. Omatsu, Y., et al., *The essential functions of adipo-osteogenic progenitors as the*
1054 *hematopoietic stem and progenitor cell niche.* Immunity, 2010. **33**(3): p. 387-99.
1055 30. Agarwal, P., et al., *Mesenchymal Niche-Specific Expression of Cxcl12 Controls*
1056 *Quiescence of Treatment-Resistant Leukemia Stem Cells.* Cell Stem Cell, 2019. **24**(5):
1057 p. 769-784 e6.
1058 31. Baccin, C., et al., *Combined single-cell and spatial transcriptomics reveal the*
1059 *molecular, cellular and spatial bone marrow niche organization.* Nat Cell Biol, 2020.
1060 **22**(1): p. 38-48.
1061 32. Wolock, S.L., et al., *Mapping Distinct Bone Marrow Niche Populations and Their*
1062 *Differentiation Paths.* Cell Rep, 2019. **28**(2): p. 302-311 e5.
1063 33. Heydt, Q., et al., *Adipocytes disrupt the translational programme of acute*
1064 *lymphoblastic leukaemia to favour tumour survival and persistence.* Nat Commun,
1065 2021. **12**(1): p. 5507.
1066 34. Spiegel, A., et al., *Unique SDF-1-induced activation of human precursor-B ALL cells as*
1067 *a result of altered CXCR4 expression and signaling.* Blood, 2004. **103**(8): p. 2900-7.
1068 35. Shafat, M.S., et al., *Leukemic blasts program bone marrow adipocytes to generate a*
1069 *protumoral microenvironment.* Blood, 2017. **129**(10): p. 1320-1332.
1070 36. Mukohira, H., et al., *Mesenchymal stromal cells in bone marrow express adiponectin*
1071 *and are efficiently targeted by an adiponectin promoter-driven Cre transgene.* Int
1072 Immunol, 2019. **31**(11): p. 729-742.
1073 37. Zhang, Z., et al., *Bone marrow adipose tissue-derived stem cell factor mediates*
1074 *metabolic regulation of hematopoiesis.* Haematologica, 2019. **104**(9): p. 1731-1743.
1075 38. Germain, P.L., et al., *Doublet identification in single-cell sequencing data using*
1076 *scDblFinder.* F1000Res, 2021. **10**: p. 979.
1077 39. Aran, D., et al., *Reference-based analysis of lung single-cell sequencing reveals a*
1078 *transitional profibrotic macrophage.* Nat Immunol, 2019. **20**(2): p. 163-172.
1079 40. Kolberg, L., et al., *gprofiler2 -- an R package for gene list functional enrichment*
1080 *analysis and namespace conversion toolset g:Profiler.* F1000Res, 2020. **9**.
1081 41. Schubert, M., et al., *Perturbation-response genes reveal signaling footprints in cancer*
1082 *gene expression.* Nat Commun, 2018. **9**(1): p. 20.
1083 42. Gulati, G.S., et al., *Single-cell transcriptional diversity is a hallmark of developmental*
1084 *potential.* Science, 2020. **367**(6476): p. 405-411.
1085 43. Jin, S., et al., *Inference and analysis of cell-cell communication using CellChat.* Nat
1086 Commun, 2021. **12**(1): p. 1088.
1087 44. De Falco, A., et al., *A variational algorithm to detect the clonal copy number*
1088 *substructure of tumors from scRNA-seq data.* Nat Commun, 2023. **14**(1): p. 1074.
1089 45. Brady, S.W., et al., *The genomic landscape of pediatric acute lymphoblastic leukemia.*
1090 Nat Genet, 2022. **54**(9): p. 1376-1389.
1091 46. Malard, F. and M. Mohty, *Acute lymphoblastic leukaemia.* Lancet, 2020. **395**(10230):
1092 p. 1146-1162.
1093 47. Li, R., et al., *Detection of cell markers from single cell RNA-seq with sc2marker.* BMC
1094 Bioinformatics, 2022. **23**(1): p. 276.
1095